



**HAL**  
open science

## The PROSCOOP10 gene encodes two extracellular hydroxylated peptides and impacts flowering time in *Arabidopsis*

Marie-Charlotte Guillou, Thierry Balliau, Emilie Vergne, Hervé Canut, Josiane Chourré, Claudia Herrera-León, Francisco Ramos-Martín, Masoud Ahmadi-Afzadi, Nicola D'amelio, Eric Ruelland, et al.

### ► To cite this version:

Marie-Charlotte Guillou, Thierry Balliau, Emilie Vergne, Hervé Canut, Josiane Chourré, et al.. The PROSCOOP10 gene encodes two extracellular hydroxylated peptides and impacts flowering time in *Arabidopsis*. 2022. hal-03915560v1

**HAL Id: hal-03915560**

**<https://ut3-toulouseinp.hal.science/hal-03915560v1>**

Preprint submitted on 6 Oct 2022 (v1), last revised 23 Jan 2023 (v2)

**HAL** is a multi-disciplinary open access archive for the deposit and dissemination of scientific research documents, whether they are published or not. The documents may come from teaching and research institutions in France or abroad, or from public or private research centers.

L'archive ouverte pluridisciplinaire **HAL**, est destinée au dépôt et à la diffusion de documents scientifiques de niveau recherche, publiés ou non, émanant des établissements d'enseignement et de recherche français ou étrangers, des laboratoires publics ou privés.

Copyright

# 1 The *PROSCOOP10* gene encodes two extracellular hydroxylated peptides and 2 impacts flowering time in Arabidopsis

3  
4 Marie-Charlotte Guillou<sup>1</sup>, Thierry Balliau<sup>2</sup>, Emilie Vergne<sup>1</sup>, Hervé Canut<sup>3</sup>, Josiane Chourré<sup>3</sup>, Claudia  
5 Herrera-León<sup>4</sup>, Francisco Ramos-Martín<sup>4</sup>, Masoud Ahmadi-Afzadi<sup>1,5</sup>, Nicola D'Amelio<sup>4</sup>, Eric Ruelland<sup>6</sup>,  
6 Michel Zivy<sup>2</sup>, Jean-Pierre Renou<sup>1</sup>, Elisabeth Jamet<sup>3</sup>, Sébastien Aubourg<sup>1\*</sup>.

7  
8 <sup>1</sup> Univ Angers, Institut Agro, INRAE, IRHS, SFR QUASAV, F-49000, Angers, France

9 <sup>2</sup> Université Paris-Saclay, INRAE, CNRS, AgroParisTech, GQE - Le Moulon, PAPPISO, F-91190, Gif-sur-Yvette, France

10 <sup>3</sup> Laboratoire de Recherche en Sciences Végétales, Université de Toulouse, CNRS, UPS, Toulouse INP, F-31320,  
11 Auzeville-Tolosane, France

12 <sup>4</sup> Unité de Génie Enzymatique et Cellulaire UMR 7025 CNRS, Université de Picardie Jules Verne, F-80039, Amiens,  
13 France

14 <sup>5</sup> Department of Biotechnology, Institute of Science and High Technology and Environmental Sciences, Graduate  
15 University of Advanced Technology, Kerman, Iran

16 <sup>6</sup> Université de Technologie de Compiègne, Unité de Génie Enzymatique et Cellulaire UMR 7025 CNRS, F-60203,  
17 Compiègne, France

18

19 Correspondence: 42 rue Georges Morel, 49070 BEAUCOUZE, FRANCE, +33 (0)2 41 22 57 40

20

21 [marie-charlotte.guillou@inrae.fr](mailto:marie-charlotte.guillou@inrae.fr); [thierry.balliau@inrae.fr](mailto:thierry.balliau@inrae.fr); [emilie.vergne@inrae.fr](mailto:emilie.vergne@inrae.fr);

22 [herve.canut@cnrs.fr](mailto:herve.canut@cnrs.fr); [chourre@lrsv.ups-tlse.fr](mailto:chourre@lrsv.ups-tlse.fr); [claudia.herrera@u-picardie.fr](mailto:claudia.herrera@u-picardie.fr); [23 \[picardie.fr\]\(mailto:picardie.fr\); \[masoud.ahmadi-afzadi@inrae.fr\]\(mailto:masoud.ahmadi-afzadi@inrae.fr\); \[nicola.damelio@u-picardie.fr\]\(mailto:nicola.damelio@u-picardie.fr\); \[eric.ruelland@utc.fr\]\(mailto:eric.ruelland@utc.fr\);](mailto:francisco.ramos@u-</a></p></div><div data-bbox=)

24 [michel.zivy@inrae.fr](mailto:michel.zivy@inrae.fr); [jean-pierre.renou@inrae.fr](mailto:jean-pierre.renou@inrae.fr); [jamet@lrsv.ups-tlse.fr](mailto:jamet@lrsv.ups-tlse.fr); [sebastien.aubourg@inrae.fr](mailto:sebastien.aubourg@inrae.fr)

25

26 Submission Date : 06/09/2022

27 6 figures, 1 table, 8 supplementary tables, 7 supplementary figures, 5252 words (start of the  
28 introduction to the end of the acknowledgements, excluding materials and methods)

## 29 HIGHLIGHT

30 The *PROSCOOP10* gene encodes two post-translationally modified extracellular SCOOP10  
31 peptides and acts upstream of *SOC1* and *LFY* to delay flowering.

## 32 RUNNING TITLE

33 Characterization of native SCOOP10 peptides and action of *PROSCOOP10* on floral transition

## 34 ABSTRACT

35 The Arabidopsis *PROSCOOP* genes belong to a family predicted to encode secreted pro-  
36 peptides which undergo maturation steps to produce peptides named SCOOP. Some of them  
37 are involved in defence signalling through their perception by a receptor complex including  
38 MIK2, BAK1 and BKK1. Here, we focused on the *PROSCOOP10* gene which is highly and  
39 constitutively expressed in the aerial organs. The MS/MS analyses of leaf apoplastic fluids  
40 allowed the identification of two distinct peptides, named SCOOP10#1 and SCOOP10#2,

41 covering two different regions of PROSCOOP10. They both possess the canonical S-X-S  
42 family motif and have hydroxylated prolines. This identification in apoplastic fluids confirms for  
43 the first time the biological reality of SCOOP peptides. NMR and molecular dynamics studies  
44 showed that the SCOOP10 peptides, although largely unstructured in solution, tend to assume  
45 a hairpin-like fold exposing the two serine residues previously identified as essential for the  
46 peptide activity. Furthermore, *PROSCOOP10* mutations led to an early flowering phenotype  
47 and an increased expression of the floral integrators *SOC1* and *LEAFY*, consistent with the  
48 transcription of *PROSCOOP10* in several mutants displaying an early or late flowering  
49 phenotype. These results suggest a role of *PROSCOOP10* in flowering time, illustrating the  
50 functional complexity of the *PROSCOOP* family.

51 **Keywords:** phyto cytokine, apoplasm, post-translational modification, flowering, Arabidopsis,  
52 peptidomics

## 53 INTRODUCTION

54 Small secreted peptides originate from the processing of protein precursors that share a N-  
55 terminal signal peptide addressing them to the secretory pathway. We distinguish (i) small  
56 post-translationally modified peptides (PTMPs) that are produced by proteolytic processing  
57 (Murphy *et al.*, 2012); and (ii) cysteine-rich peptides (CRPs) characterised by an even number  
58 of cysteine residues involved in intramolecular disulfide bonds (Matsubayashi, 2011;  
59 Tavormina *et al.*, 2015). An integrative approach combining bioinformatics, transcriptomics and  
60 phenotyping has led to the identification of a gene family encoding precursors of putative small  
61 PTMPs named Serine-riCh endOgenOus Peptides (SCOOPs) (Gully *et al.*, 2019). All the  
62 predicted SCOOP peptides share a S-X-S motif and are specific to the *Brassicaceae* species.  
63 Moreover, assays based on application of synthetic peptides have shown that SCOOP  
64 peptides are phyto cytokines involved in defence signalling through their perception by the  
65 MDIS1-INTERACTING leucine-rich repeat receptor kinase 2 (MIK2) (Hou *et al.*, 2021; Rhodes  
66 *et al.*, 2021) and the two co-receptors BRI1-associated receptor kinase (BAK1) and BAK1-  
67 LIKE 1 (BKK1) (Gully *et al.*, 2019; Hou *et al.*, 2021; Rhodes *et al.*, 2021). New studies tolerating  
68 a greater variability in the C-terminal motif of the PROSCOOP amino acid sequence have  
69 expanded the SCOOP family to 28 members (Zhang *et al.*, 2022). For example, the  
70 SECRETED TRANSMEMBRANE PEPTIDE family (STMP) contains 10 members out of which  
71 four were also annotated as SCOOP peptides: STMP1, STMP2, STMP8 and STMP10  
72 correspond actually to SCOOP13, SCOOP14, SCOOP15 and SCOOP4 respectively (Yu *et al.*,  
73 2019). Additionally, the ENHANCER OF VASCULAR WILT RESISTANCE 1 peptide  
74 (EWR1) and four closely related peptides also encode functional SCOOP peptides (Zhang *et al.*,  
75 2022). All these peptides share the SCOOP characteristics and can induce MIK2-

76 dependent immune responses. However, the transcription profiles of the *PROSCOOP* genes  
77 are contrasted according to organs and various stimuli. This raises the question of the  
78 involvement of the SCOOP peptides in different biological functions, notably in plant  
79 development. Indeed, *PROSCOOP12* (*AT5G44585*) is constitutively expressed in roots and  
80 recent studies have shown that SCOOP12 is a moderator of root elongation through the control  
81 of reactive oxygen species (ROS) homeostasis (Guillou *et al.*, 2022). This study focuses on  
82 *PROSCOOP10* (*AT5G44580*) which is highly expressed in the aerial parts. We show that  
83 *PROSCOOP10* encodes a propeptide which gives rise to two distinct peptides that we have  
84 identified in leaf apoplastic fluids. We identify a tendency of hairpin structure of these peptides  
85 exposing the S-X-S SCOOP motif. Then, we also show an early flowering phenotype in  
86 *proscop10* mutants suggesting a role in the development of the aerial part of the plant and  
87 particularly in flowering time.

88

## 89 **MATERIALS AND METHODS**

### 90 **Plant material**

91 *Arabidopsis thaliana* ecotype Columbia (Col-0) was used as control. Two independent  
92 *proscop10* mutant lines in the Col-0 background were used. A first line, named *proscop10-*  
93 *1*, was a T-DNA insertion line obtained from NASC (SALK\_059855C) and the primers used for  
94 genotyping are listed in **Supplementary Table S1**. T-DNA insertion was checked by PCR on  
95 *PROSCOOP10* and compared with PCR on *AtCOP1*, used as a PCR positive control, in Col-  
96 0 and *proscop10-1* mutant line. The second line, named *proscop10-2*, was created using  
97 the CRISPR/Cas9 (clustered regularly interspaced short palindromic repeats/CRISPR-  
98 associated protein 9) method. We searched for *PROSCOOP10*-specific single guide RNA  
99 (sgRNA) and checked possible off target sites in the *Arabidopsis* Col-0 genome using the  
100 Crispor Tefor program (<http://crispor.tefor.net>). The 20-base long RNA guides with the  
101 following sequences were used: 5'-GACCACGCTCCAGGCAGTAA-3' and 5'-  
102 ATCAGGCAGTGGGCATGGTG-3' (**Supplementary Fig. S1A**). Vectors and methods to get  
103 the CRISPR/Cas9 constructs were as in Charrier *et al.* (2019). *Arabidopsis* transformation was  
104 applied as in Zang *et al.* (2006).

105 The soil-grown plants used for ROS assay and phenotyping were grown under long-day  
106 conditions (16 h light at 22 °C/16 h dark at 21 °C, 70% relative humidity). Seedlings used for  
107 seedling growth inhibition assay were grown under short-day conditions (8 h light at 22 °C/8 h  
108 dark at 21 °C, 70% relative humidity). Plants used for mass spectrometry (MS) analysis were  
109 cultivated on soil under short-day conditions (8 h light at 22 °C/16 h dark at 21 °C, 70% relative

110 humidity) during four weeks. Sodium and mercury vapor lights were used providing a light  
111 intensity of  $352.9 \mu\text{mol.m}^{-2}.\text{s}^{-1}$ .

## 112 **Synthetic peptides**

113 The following peptides: flg22 (QRLSTGSRINSAKDDAAGLQIA), SCOOP12  
114 (PVRSSQSSQAGGR), SCOOP10#1 (SAIGTOSSTSDHAOGSNG), SCOOP10#2  
115 (GDIFTGOSGSGHGGGRTOAP) were obtained from GeneCust (Boynes, France), O  
116 corresponding to hydroxyprolines. SCOOP10#2\* (GDIFTGPSGSGHGGGRTPAP)  
117 corresponding to SCOOP10#2 without hydroxyprolines was obtained from Eurogentec SA  
118 (Seraing, Belgium). Peptides were synthesized with a minimum purification level of 95% and  
119 diluted in water to the final concentration used for the assays. The SCOOP10#1 and  
120 SCOOP10#2 peptide sequences were identical to the native sequences identified by mass  
121 spectrometry.

122

## 123 **Mass Spectrometry (MS) analyses of extracellular fluids**

124 The extracellular fluids of rosettes were obtained according to Boudart *et al.* (2005) with slight  
125 modifications. The buffer used for the vacuum infiltration contained 5 mM sodium acetate at  
126 pH 4.6, with or without 0.3 M mannitol, and three protease inhibitors: 1 mM AEBSF  
127 (ThermoFisher, Scientific, Rockford, IL, USA), 10 mM 1-10 phenanthroline (Sigma Aldrich  
128 Chimie SARL, Saint-Quentin-Fallavier, France), and 100  $\mu\text{M}$  E64 (Sigma-Aldrich). After  
129 centrifugation at 200 *g* of the vacuum-infiltrated rosettes, the fluids were collected and  
130 submitted to an ultrafiltration using an Amicon® Ultra 10K device — 10,000 NMWL (Merck  
131 Chimie SAS, Darmstadt, Germany). The samples were then speedvac-dried prior to  
132 solubilization in 10 mM DTT and 50 mM ammonium bicarbonate, followed by alkylation with  
133 50 mM iodoacetamide. The samples were directly desalted by solid phase extraction (SPE) on  
134 C18 cartridges (StrataTM-XL 8E-S043-TG, Phenomenex, Le Pecq, France) as described in  
135 Balliau *et al.* (2018). Alternatively, the samples were subjected to tryptic digestion inside the  
136 cartridge. The peptides were eluted with 70% acetonitrile/0.06% acetic acid prior to be  
137 speedvac-dried. They were finally resuspended in 2% acetonitrile/0.1% formic acid. The  
138 samples were analysed by MS with a Q ExactiveTM-Plus Hybrid Quadrupole-Orbitrap™ mass  
139 spectrometer (Thermo-Fisher Scientific, Waltham, MA, USA) coupled with an Eksigent  
140 NanoLC-Ultra® 2D HPLC (AB SCIEXTM, Redwood City, CA, USA) as described (Balliau *et*  
141 *al.*, 2018), except for the chromatographic separation step that was shortened to 45 min.  
142 Database search was performed as described (Duruflé *et al.*, 2019), except for the enzymatic  
143 cleavage that was specified to “no enzyme”. Protein inference was performed using the

144 X!TandemPipeline (Langella *et al.*, 2017) with the following parameters: peptide E-value  
145 smaller than 0.003, protein E-value smaller than 0.01, and one peptide per protein.

146

### 147 **Nuclear Magnetic Resonance (NMR) analyses**

148 SCOOP synthetic peptides were dissolved at concentrations between 0.5 mM and 1 mM in  
149 both 50 mM phosphate buffer water solution, pH 6.6, containing 10% D<sub>2</sub>O and in DMSO-d<sub>6</sub>.  
150 Deuterated sodium TSP-d<sub>4</sub> at a concentration of 100 μM was used as an internal reference  
151 for chemical shift in aqueous buffers (Wishart *et al.*, 1995). Measurements were performed at  
152 278 K for aqueous and at 298 K for DMSO samples. Almost complete assignment of amide  
153 protons, non-exchanging protons and protonated <sup>13</sup>C atoms was achieved in solution by  
154 <sup>1</sup>H,<sup>13</sup>C-HSQC, <sup>1</sup>H,<sup>1</sup>H-TOCSY (mixing time of 60 ms), and <sup>1</sup>H,<sup>1</sup>H-NOESY (mixing time of 200  
155 ms) recorded on a 500 MHz (11.74 T) Bruker spectrometer (Bruker France, Palaiseau)  
156 equipped with a 5 mm BBI (Broadband Inverse) probe. TopSpin 4 (Bruker BioSpin) and  
157 NMRFAM-SPARKY (Lee *et al.*, 2015) were used to process and to analyse NMR data.  
158 Chemical shift deviations from random coil values were calculated using the “secondary  
159 chemical shift analysis” option of NMRFAM-SPARKY (Lee *et al.*, 2015), a module based on  
160 PACSY (Lee *et al.*, 2012).

161

### 162 **Molecular Dynamics (MD) simulations**

163 The starting structures for our peptides were obtained by I-Tasser (Yang *et al.*, 2015). *In silico*  
164 mutagenesis was performed in CHIMERA using the Rotamers tool (Pettersen *et al.*, 2004).  
165 The proline residues were replaced by hydroxyproline residues using YASARA (Krieger *et al.*,  
166 2014). The GROMACS package v5.0.7 (Abraham *et al.*, 2015) was used to run MD  
167 simulations. The AMBER99SB-ILDN (Lindorff-Larsen *et al.*, 2010) force field was used to  
168 provide molecular mechanics parameters to our peptides. The peptides were put in a cubic  
169 cell (“box”), the border of which is at least 1 nm from the protein, and we solvate it with TIP3P  
170 explicit water molecules. Counterions were added, if necessary, to obtain a neutral system and  
171 took the place of water molecules. Energy minimization and the temperature and pressure  
172 equilibrations were done as described in Pokotylo *et al.*(2020). The equilibration time was also  
173 set at 100 ps relaxation time. Once our peptide was well-equilibrated at the desired  
174 temperature (300 K) and pressure (1 bar), we released the position restraints and run  
175 production MD for data collection. The peptides were subjected to 500 ns simulation with 2 fs  
176 time steps. To evaluate the reproducibility, the whole process (minimization, equilibration and  
177 production run) was repeated thrice. PyMol (DeLano *et al.*, 2002) and VMD (Humphrey *et al.*,

178 1996) were used for visualisation. Graphs and images were created with GNUplot (Janert *et*  
179 *al.*, 2010) and PyMol (DeLano *et al.*, 2002). All MD trajectories were analysed using  
180 GROMACS tools (Smith *et al.*, 2010; Lemkul *et al.*, 2018) along the last 250 ns. Polar contacts  
181 maps were determined by calculating the radial distribution function of each nitrogen and  
182 oxygen atom from all others and taking its maximum intensity in the range of H-bonds and salt-  
183 bridges. This allows to have an overview of all polar interatomic interactions and their  
184 occurrence (Ramos-Martin *et al.*, 2020).

185

### 186 **Seedling growth inhibition assay**

187 Seedlings were germinated on MS (1X) agar (1%) and grown for five days before transferring  
188 one seedling per well of 24-well plates containing 500  $\mu$ L of MS medium or MS medium  
189 supplied with the indicated elicitor peptide to a final concentration of 1  $\mu$ M (six replicates per  
190 elicitor peptide treatment). Fresh masses were measured and the experiment was repeated  
191 thrice.

192

### 193 **ROS assay**

194 ROS production was determined by a luminol-based assay. Three five-week old seedlings  
195 grown on MS plates were incubated in 200  $\mu$ L double distilled water (ddH<sub>2</sub>O) overnight in a 1.5  
196 mL centrifuge tube. Then, ddH<sub>2</sub>O was replaced by 200  $\mu$ L of reaction solution containing 100  
197  $\mu$ M of luminol and 10  $\mu$ g/mL of horseradish peroxidase (Sigma-Aldrich, Saint-Louis, USA)  
198 supplemented with or without 1  $\mu$ M peptide. Luminescence was measured for 60 min with a  
199 one-second interval, immediately after adding the solution with a FLUOstar OPTIMA plate  
200 reader (BMG LABTECH, Ortenberg, Germany). The total values of ROS production were  
201 indicated as means of the relative light units (RLUs).

202

### 203 **Gene expression analysis**

204 For each of the three biological repetitions, shoot apical meristem (SAMs) samples were hand-  
205 dissected under binocular magnifier, trying to remove as much leaf tissue as possible, from 15  
206 individual 7 and 11-day old plants of Col-0, *proscop10-1* and *proscop10-2*, growing under  
207 long-day conditions. Total RNAs were extracted using the Nucleospin RNA Plus Kit  
208 (Macherey-Nagel, Düren, Germany). cDNAs were synthesized from 1.5  $\mu$ g of total RNA with  
209 oligo(dT) primers using Moloney Murine Leukemia Virus Reverse Transcriptase MMLV-RT  
210 according to the manufacturer's instructions (Promega, Madison, WI, USA). RT-qPCR was

211 carried out in a Chromo4 system (Bio-Rad, Laboratories, CA, USA). Expression profiles of key  
212 floral transition genes were calculated using the  $2^{-\Delta\Delta Ct}$  method and were corrected as  
213 recommended in Vandesompele *et al.* (2002), with three internal reference genes (*ACT2*,  
214 *COP1* and *AP4M*) used for the calculation of a normalization factor. Mean expression level of  
215 Col-0 at 7 days served as calibrator. Primers for RT-qPCR analysis used are specified in  
216 **Supplementary Table S1**.

217

## 218 **RESULTS**

### 219 **Identification of SCOOP10 peptides in extracellular fluids by MS**

220 Based on the high expression level of *PROSCOOP10* in leaves, we used a proteomic  
221 approach to explore the apoplastic fluid content and search for the native form(s) of SCOOP10.  
222 The experiment has been repeated thrice, twice without mannitol in the infiltration buffer and  
223 once in the presence of 0.3 M mannitol. The results were similar. In one case, a tryptic digestion  
224 of the proteins has been performed prior to the MS analysis. Different peptides could be  
225 identified covering two different regions of PROSCOOP10: they are indicated as SCOOP10#1  
226 and SCOOP10#2 in **Fig. 1**. The corresponding MS/MS spectra are shown in **Supplementary**  
227 **Fig. S2**. The native SCOOP10#1 peptide comprises 18 amino acids and it covers the central  
228 predicted conserved motif defined after the comparison of the amino acid sequences of the  
229 members of the PROSCOOP family (Gully *et al.*, 2019): SAIGTPSSTSDHAPGSNG (**Fig. 1A,**  
230 **B**). It contains the two strictly conserved serine (S) residues. All the observed peptides are  
231 native ones, as shown by the absence of tryptic sites at their N- and C-termini. SCOOP10#1  
232 was only observed thrice compared to the 38 observations of SCOOP10#2. In all these three  
233 occurrences, it contained two hydroxyproline (O) residues. The native SCOOP10#2 peptide  
234 comprises 20 amino acids at the most and covers the C-terminal predicted conserved motif of  
235 the PROSCOOP family (Gully *et al.*, 2019): GDIFTGPSGSGHGGGRTAP (**Fig. 1A, C**). As  
236 SCOOP10#1, it also contains the two strictly conserved serine residues. It also carries three  
237 well-conserved successive glycine (G) residues. The C-terminus observed at arginine (R)16  
238 in ten cases resulted from tryptic digestion and the corresponding peptides should not be  
239 considered as native ones. All the other observed peptides are native ones because they are  
240 not surrounded by tryptic sites. Contrary to SCOOP10#1, the pattern of proline (P)  
241 hydroxylation is variable: We could observe hydroxyproline residues at either of the three  
242 possible positions (P7, P18 or P20) and in various combinations (**Fig. 1B**). The most frequently  
243 observed position of P hydroxylation was P18 (65.8%), followed by P7 (36.8%). In some cases,  
244 P hydroxylation was observed at two positions on the same peptide: P7 and P18 (23.7%) or  
245 P7 and P20 (7.9%). The C-terminus of the peptide was variable ending with P18, alanine A19

246 or P20. Although protease inhibitors are used already at the beginning of the experiment, the  
247 variability of the C-terminus could be due to proteolysis by serine carboxypeptidases identified  
248 in cell wall proteomes (see *WallProtDB-2*, San Clemente and Jamet, 2015; San Clemente *et*  
249 *al.*, 2022).

250

## 251 **SCOOP10#2 is unstructured in solution but cis-trans isomerization may be favoured in** 252 **a hydrophobic environment**

253 According to MS analyses, SCOOP10#2 seems to be the major secreted or the more stable  
254 peptide produced by *PROSCOOP10*. Therefore, now knowing its exact sequence, we decided  
255 to study its structural behaviour in solution, using a hydroxylated synthetic SCOOP10#2  
256 peptide (GDIFTGOSGSGHGGGRTOAP) and a non-hydroxylated one, SCOOP10#2\*  
257 (GDIFTGPSGSGHGGGRTPAP).

258 NMR data indicated that the synthetic SCOOP10#2 peptide is largely unstructured in water  
259 solution. The NMR assignment of both non-hydroxylated (SCOOP10#2\*) and hydroxylated  
260 (SCOOP10#2) forms are reported in **Supplementary Tables S2 and S3**, respectively. The  
261 chemical shift of some nuclei, namely H $\alpha$ , C $\alpha$ , C $\beta$  and carbonyl, can be used to ascertain the  
262 presence of secondary structure by observing their deviations from random coil values  
263 (Wishart *et al.*, 1992; Wishart *et al.*, 1994; Wishart *et al.*, 2011) which can be predicted by the  
264 peptide sequence (Nielsen *et al.*, 2018). The H $\alpha$ /C $\alpha$  region of the  $^1\text{H}$ ,  $^{13}\text{C}$ -HSQC NMR spectrum  
265 is shown in **Fig. 2A**, while the chemical shift deviations from random coil values are reported  
266 in **Fig. 2B**. The presence of alpha helical structure can be monitored by at least three  
267 consecutive negative H $\alpha$ , C $\beta$  or positive C $\alpha$  deviations while the opposite holds for beta  
268 strands. The difference between C $\alpha$  and C $\beta$  deviations is often used as a combined predictor.  
269 Overall, the observed deviations are below the threshold value of 0.1 ppm for  $^1\text{H}$  and 0.7 ppm  
270 for  $^{13}\text{C}$  (Wang *et al.*, 2002). Hydroxylation of P7 and P18 has no major impact on the structure  
271 as indicated by minimal chemical shift perturbations on most resonances (**Fig. 2A**). Large  
272 changes are limited to the atoms of hydroxyprolines (O) and particularly to C $\gamma$  carbon atoms  
273 as expected.

274 NMR spectra also allowed monitoring the conformation of the peptide bond linking proline  
275 residues to the previous amino acid (Dorman *et al.*, 1973; Siemon *et al.*, 1975). Such bond can  
276 often assume *cis* conformation whereas it is commonly found *trans* in all other amino acid  
277 types (Wedemeyer *et al.*, 2002). A *cis* conformation determines a rather radical change in the  
278 direction of the peptide backbone and might be crucial for the biological function. In particular,  
279 the H $\alpha$  of the preceding residue is close in space to the H $\alpha$  or H $\delta$  protons of proline in the *cis*  
280 and *trans* conformation, respectively. Its resonance can therefore be used to identify each

281 conformer in NOESY or ROESY spectra (Gaggelli *et al.*, 2001). A clear NOESY peak between  
282 the H $\alpha$  protons of G6 and H $\delta$  protons of P7 (or O7) revealed that the peptide bond is mainly in  
283 *trans* conformation.

284 In order to investigate the structural behaviour of SCOOP10#2 in a more apolar environment  
285 which could mimic that of its receptor, we studied the peptide in DMSO (**Supplementary Fig.**  
286 **S3 and Supplementary Tables S4 and S5**). Interestingly, we observed a doubling of peaks  
287 arising from residues 6-10, which is the region comprising the two conserved serine residues  
288 (**Fig. 1A**). Analysis of NOESY spectra reveals that the minor form might belong to the *cis*  
289 conformation of the G6-P7 peptide bond, as a cross peak is present between the H $\alpha$  proton of  
290 G6 and an H $\alpha$  compatible with a second form of P7. The same was not observed for P18 and  
291 P20.

292

### 293 **Transient hairpin-like structures exposing S8 and S10 might have functional relevance**

294 Molecular dynamics simulations also pointed at the absence of a well-defined structure in both  
295 SCOOP10#2\* and its hydroxylated form, in agreement with NMR data. Indeed, during MD  
296 simulations, an ensemble of different conformations continuously interconverted along the  
297 trajectory (**Fig. 3A**). However, these data revealed a certain tendency of the backbone to fold  
298 at the level of residues O7-S10, thus exposing S8 and S10 side chains. Interestingly, this  
299 region is the one displaying negative H $\alpha$  and positive C $\alpha$ -C $\beta$  deviations in NMR, as expected  
300 for the turn of a helix (**Fig. 3B**). Although below the threshold values, these data suggest the  
301 presence of a small population of conformers contributing to the average chemical shift value.  
302 For this reason, we analysed molecular dynamic trajectories, in order to reveal key interatomic-  
303 interactions that might stabilise such a fold. For SCOOP10#2, the obtained polar contacts map  
304 reveals the formation of an H-bond between the amide nitrogen of serine S10 and the carbonyl  
305 of hydroxyproline O7 (**Fig. 3C**) or proline P7 (data not shown), a salt bridge between the side  
306 chains of aspartic acid D2 and arginine R16, and a salt bridge between the C- and N-termini  
307 (**Fig. 3D**). Furthermore, a stacking between the aromatic rings of phenylalanine F4 and  
308 histidine H12 might also further stabilise the conformation (**Fig. 3D**). Similar contacts are  
309 observed in the non-hydroxylated form (data not shown).

310 In order to test the relative contribution of each of these key inter-residue interactions we  
311 performed multiple molecular dynamic simulations where we mutated at least one partner  
312 residues: R16A, G13,14,15A, P7A and S8,10A (**Supplementary Figure S4A**). In the R16A  
313 mutant, where we eliminated the salt bridge between D2 and R16, SCOOP10#2\* still tends to  
314 fold onto itself but at the level of residues 12-15 (**Supplementary Figure S4B**), thus reducing  
315 the exposition of S8 (**Supplementary Figure S5**). In this case the driving force is the salt

316 bridge between the N and C termini. When glycine residues in the flexible region G13,14,15  
317 are mutated to alanine, the N-C terminal interaction favours a fold in the middle of the structure  
318 (residues 9-10) (**Supplementary Fig. S4B**). As for the H-bond between the amide of S10 and  
319 P7, mutants (P7A and double mutant S8,10A) reveal small perturbation of the structural  
320 behaviour (in P7A the structure folds around residue 8 by a turn rather than a helix 3-10), an  
321 effect somehow expected considering that the interaction is established at the level of the  
322 backbone.

323

### 324 **SCOOP10#1 is unstructured in solution with transient head-to-tail contact**

325 We also studied the structural behaviour in solution of SCOOP10#1, using a synthetic  
326 SCOOP10#1 peptide identical to the native form identified (SAIGTOSSTSDHAOGSNG). For  
327 the synthetic SCOOP10#1 peptide, deviations from random coil values also indicate a poor  
328 structuring (**Supplementary Fig. S6**, and the NMR assignment in different conditions in  
329 **Supplementary Tables S6 and S7**), and NOESY spectra are compatible with *trans*  
330 conformation for the peptide bonds involving both P6 and P14. Contrarily to what observed for  
331 SCOOP10#2, we could not detect the presence of *cis* conformation in the more apolar  
332 environment of DMSO. MD simulations (**Supplementary Fig. S7**) agree with NMR data and  
333 detect lack of structure (**Supplementary Fig. S7A**), however, infrequent contacts between the  
334 N- and C-termini (**Supplementary Fig. S7B**) generate folded conformations vaguely  
335 resembling those observed for SCOOP10#2 (see contact map in **Supplementary. Fig. S7C**).

336

### 337 **SCOOP10 peptides do not induce ROS production and growth inhibition**

338 Effects of the SCOOP10 synthetic peptides on seedling growth and ROS production were  
339 tested on Col-0 and *mik2-1* genotypes and compared to those of the SCOOP12 peptide, as a  
340 control (**Fig. 4**). The SCOOP12 amino acid sequence was the same already used by Gully *et*  
341 *al.* (2019) and Guillou *et al.* (2022) and based on prediction without post-translational  
342 modifications.

343 In Col-0 background and at 1  $\mu$ M, we showed that, the SCOOP10#2\* peptide induced a  
344 seedling growth inhibition which was much smaller than that induced by the SCOOP12 peptide.  
345 In the same conditions, the SCOOP10#1 and SCOOP10#2 peptides did not show a significant  
346 effect. In the *mik2-1* mutant background, none of the SCOOP peptides had an effect on growth,  
347 as expected (**Fig. 4A**). At the same concentration, the SCOOP12 peptide induced a strong  
348 ROS production in Col-0 leaves, as already reported (Gully *et al.*, 2019; Rhodes *et al.*, 2021).  
349 On the contrary, neither the SCOOP10#2\* nor the SCOOP10#1 and the SCOOP10#2

350 peptides, even simultaneously applied, induce ROS production in leaves. As expected none  
351 of the SCOOP peptides induced a high ROS production in the *mik2-1* mutant (**Fig. 4B**).

352

### 353 **Mutations of *PROSCOOP10* impact flowering time**

354 Previous analysis of transcriptomic data showed that *PROSCOOP10* is highly expressed in  
355 shoot apex and leaves and may play a role in aerial organ development (Gully *et al.*, 2019;  
356 Hou *et al.*, 2021). Therefore, we compared the leaf development and flowering time of wild-  
357 type and *proscop10* plants. The first *proscop10* mutant (*proscop10-1*) is a T-DNA insertion  
358 line ordered from NASC (**Supplementary Fig. S1A**). This line was genotyped as mutated on  
359 both DNA and cDNA (**Supplementary Fig. S1B**). We generated a second line (*proscop10-*  
360 *2*) using a CRISPR/Cas9 approach and the mutant was genotyped (**Supplementary Fig. S1C,**  
361 **D**). *proscop10-2* was a bi allelic mutant, which is frequently observed with this approach  
362 (Pauwels *et al.*, 2018). In the first modified allele, a deletion of 237 bp occurred between the  
363 two guides in addition to modifications of nucleotides within the guides, leading to a frameshift.  
364 For the second modified allele, a deletion of 448 bp occurred between the two guides  
365 (**Supplementary Fig. S1E**). In each case, the modifications prevented the synthesis of the  
366 native SCOOP10 peptides (**Supplementary Fig. S1F**).

367 Both mutant lines displayed a normal vegetative development but 22 days after germination,  
368 the inflorescences of *proscop10* mutants bolted significantly earlier than those of Col-0 plants,  
369 with a shift of two days (**Fig. 5A, C**) and the number of rosette leaves were significantly lower  
370 for *proscop10* at bolting day (**Fig. 5E**). Consequently, five days after, mutants had longer  
371 stem length compared to Col-0 (**Fig. 5B**). 80% of the inflorescence of *proscop10* mutants  
372 bolted around the 22<sup>nd</sup> day after germination whereas the inflorescence of wild-type bolted  
373 gradually from the 23<sup>rd</sup> to the 26<sup>th</sup> day after germination (**Fig. 5D, Supplementary Table S8**).

374 Based on the mutant phenotype, we next examined the expression of three genes involved in  
375 floral regulation, *SUPPRESSOR OF CONSTANS 1* (*SOC1*), *LEAFY* and *GA3OX-1*, in the  
376 SAM of *proscop10* mutants and Col-0 at 7 and 11 days after germination (**Figure 6**). At 7  
377 days, the two floral transition genes, *SOC1* and *LEAFY*, were not differentially expressed  
378 between mutants and Col-0 whereas *GA3OX-1* was induced only in *proscop10-1*. At 11 days,  
379 all three genes were up-regulated in the two *proscop10* mutant lines compared to Col-0.

380

## 381 **DISCUSSION**

382

### 383 **Two distinct hydroxylated SCOOP10 peptides are present in the leaf apoplasm**

384 The MS analysis of apoplastic fluid samples from rosette leaves has identified two hydroxylated  
385 SCOOP10 peptides (18 and 20 aa-long) resulting from the processing of two distinct regions  
386 of the PROSCOOP10 protein separated by 10 amino acids. This result confirms that  
387 *PROSCOOP* genes are indeed encoding preproteins processed in short secreted peptides.  
388 Furthermore, the presence of hydroxyproline residues confirms that SCOOPs are PTMPs  
389 according to the Matsubayashi's classification (Matsubayashi, 2011). We thus characterized  
390 two distinct SCOOP10 peptides showing the biological reality of the previous predicted  
391 peptides SCOOP10#1 and SCOOP10#2. Note that the observed native peptides are a few  
392 amino acids longer (at both their N- and C- termini) than previously predicted. As shown by  
393 MS analyses, SCOOP10#2, corresponding to C-terminal end of the PROSCOOP10 precursor,  
394 seems to be the major form in the leave apoplasm. The ability of a precursor protein to be  
395 processed in different peptides has been described for a few genes belonging to CLE, CEP  
396 and PIP families (Murphy *et al.*, 2012; Roberts *et al.*, 2013; Vie *et al.*, 2015). In our case, the  
397 ability of *PROSCOOP10* to produce two distinct SCOOP10 peptides probably comes from the  
398 local duplication of an exon. Indeed, contrary to the large majority of *PROSCOOP* genes which  
399 have two coding exons (the first one encoding the signal peptide, and the second one  
400 containing the conserved SCOOP motif), *PROSCOOP10* has a third exon containing a second  
401 SCOOP motif (**Supplementary Fig. S1A**, Gully *et al.*, 2019). This feature is also shared by  
402 *PROSCOOP6*, *7*, *11* and *15* which are also probably able to encode two SCOOP peptides  
403 even if previous assays based on exogenous application of predicted synthetic peptides  
404 showed that only the C-terminal ones have a biological activity (Hou *et al.*, 2021; Rhodes *et al.*,  
405 2021). The identification of these native SCOOP10 peptides suggests that their maturation  
406 requires cleavage steps by endoproteases still unknown. The N-ter termini of both SCOOP10  
407 peptides are located upstream the Y[KR]PN motif (**Figure 1**) similar to the cleavage site of IDA  
408 precursors where P and Y residues in positions -2 and -4 relative to the cleaved bond are  
409 important for cleavage site recognition by subtilases SBT4.12, SBT4.13 and SBT5.2  
410 (Schardon *et al.*, 2016; Stintzi and Schaller, 2022). Because of its internal position in the  
411 precursor, the release of SCOOP10#1 probably requires additional step involving actions of  
412 another endoprotease and/or trimming by an exoprotease. Such complex maturation process  
413 has already been described for the maturation of the CLE19 peptide through the activity of the  
414 exoprotease Zn<sup>2+</sup> carboxypeptidase SOL1 in the extracellular space (Casamitjana-Martinez *et al.*,  
415 2003; Tamaki *et al.*, 2013).

416 Regarding the post-translational modifications, the SCOOP10 amino acid motifs containing the  
417 P hydroxylation sites were of three types: AP, TP, and GP. AP and TP are canonical motifs for  
418 the hydroxylation of P residues described for the CEP1 peptide (Ohyama *et al.*, 2008) and

419 arabinogalactan proteins (Showalter *et al.*, 2010; Tan *et al.*, 2003). The GP motif was found to  
420 be hydroxylated on the P residue in CLV3, CLE2 (Ohyama *et al.*, 2009), and in a few other  
421 proteins (for a review see Canut *et al.*, 2016). As previously reported for other cell wall proteins,  
422 the pattern of proline hydroxylation is variable (Duruflé *et al.*, 2017). It has been assumed that  
423 this variability could contribute to the regulation of the biological activity or play a role in  
424 recognition of the cleavage site(s) targeted by the endoproteases as Royek *et al.* (2022)  
425 demonstrated with tyrosine sulfation. At this point, our data did not allow addressing the  
426 question of the O-glycosylation of the hydroxyproline residues as reported for a few CLE  
427 peptides (Shinohara and Matsubayashi, 2010, 2013; Araya *et al.*, 2014; Takahashi *et al.*, 2018)  
428 and PSY1 (Amano *et al.*, 2007).

429 In our conditions, exogenous application of the synthetic SCOOP10#2 peptide, based on the  
430 native forms with or without hydroxylated prolines (GDIFTGOSGSGHGGRTOAP or  
431 GDIFTGPSGSGHGGRTPAP respectively), did not show any effect on seedling growth and  
432 ROS production contrary to SCOOP12 and some other members of the family. However,  
433 Rhodes *et al.* (2021) have shown that the predicted version of SCOOP10#2 peptide  
434 (FTGPSGSGHGGR) induced a slight seedling growth inhibition and a low level of ROS at 1  
435  $\mu\text{M}$  in a MIK2 dependent manner. Hou *et al.* (2021), using another predicted sequence of the  
436 SCOOP10#2 peptide (PNGDIFTGPSGSGHGGR, named SCOOP10#B in their publication),  
437 have shown that it induced both a strong seedling growth inhibition and ROS production at the  
438 same concentration and in a MIK2 dependent manner. These different results suggest that the  
439 SCOOP10#2 actions regarding ROS production and seedling growth inhibition might be  
440 sequence- and/or condition- dependent. The absence or the low effect of SCOOP10 peptides  
441 on ROS production could explain why the constitutive high level of transcription of  
442 *PROSCOOP10* in most of the aerial parts does not induce deleterious effects.

#### 443 **SCOOP10 peptides tend to adopt a hairpin structure**

444 The mature sequence of SCOOP10 peptides being known, we addressed the question of its  
445 molecular structure. NMR revealed that both synthetic SCOOP10#1 and SCOOP10#2 appear  
446 to be mainly unstructured in solution. Molecular dynamics simulations also pointed to the  
447 absence of a well-defined structure. Yet, the analysis of molecular dynamics trajectories  
448 showed that the peptides transiently adopt a hairpin conformation, especially in the case of  
449 SCOOP10#2. As often observed in ligand/receptor interactions, the active form of the protein  
450 might be scarcely populated and become major only in the presence of its target (Pucheta-  
451 Martinez *et al.*, 2016; Sekhar *et al.*, 2018). SCOOP10#2 transient structures would be  
452 stabilized by two salt-bridges. The first one, between D2 and R16 side chains, favours the  
453 formation of a turn (residues 8-9) exposing S8 and S10 while the second is between the N-

454 terminal amine and the C-terminal carboxylate. Despite the fact that the turn is not in the middle  
455 of the structure, the two salt bridges can co-exist, because the three glycine residues in position  
456 13-15 provide backbone flexibility. This stretch of glycines, located at the C-terminus of the S-  
457 X-S motif, is a feature shared by a majority of the SCOOP peptides and allows us to think that  
458 SCOOPs could adopt such a preferred conformation for the interaction with their receptor.  
459 Interestingly, this hairpin structure exposes the two conserved serine residues that define the  
460 SCOOP family and that were shown to be essential for the peptide function. Indeed, mutation  
461 of one of the two residues is fatal for SCOOP12 perception (Gully *et al.*, 2019).

462

### 463 ***PROSCOOP10* delays the floral transition**

464 The mutation of *PROSCOOP10* showed an early flowering phenotype and a lower number of  
465 leaves at bolting day compared to Col-0 plants. This observation indicates the involvement of  
466 the *PROSCOOP10* gene in flowering-time control. Multiple factors alter the flowering time such  
467 as the photoperiod, the vernalization, and the gibberellins (GAs). The pathways dependent on  
468 these factors regulate a common set of key floral integrators (Parcy *et al.*, 2004; Moon *et al.*,  
469 2005; Roux *et al.*, 2016; Li *et al.*, 2010). Among them, we tested the expression of the two major  
470 genes *SOC1* and *LEAFY* (Simpson *et al.*, 2002; Parcy *et al.*, 2005), and of *GA3OX1-3*, involved  
471 in the GA biosynthetic pathway and promoting flowering (Blázquez *et al.*, 1998). After 11 days,  
472 when the floral transition occurred (Klepikova *et al.*, 2015), all three genes were up-regulated  
473 in the two early flowering *proscoop10* mutants compared to Col-0. This suggests that  
474 *PROSCOOP10* delays flowering time by repressing the expression of *SOC1*, *LEAFY* and  
475 *GA3OX1-3*. Moreover, these results can be correlated with the *PROSCOOP10* expression  
476 profile in the aerial parts of the plant. The mining of transcriptomic data available in  
477 Genevestigator and CATdb (Zimmermann *et al.*, 2004; Gagnot *et al.*, 2008) revealed more  
478 information about the transcriptional regulation of *PROSCOOP10*. Indeed, in 2007, Moon *et al.*  
479 *al.* reported it as one of the only two genes significantly down regulated in the *pif1-5* mutant  
480 while describing the involvement of *PIF1* in the optimization of the greening process through  
481 the regulation of chlorophyll synthesis. Interestingly in 2018, Wu *et al.* also studied *PIF1* (called  
482 *PIL5*) and identified an early flowering phenotype under long day growth condition for the *pil5-*  
483 *1* mutant in which *SOC1* and *LEAFY* are also up-regulated. Moreover, Klepikova *et al.* (2015)  
484 have monitored the transcriptome of the SAM to reveal a critical time point in Arabidopsis  
485 flower initiation. In their analysis, *AT5G44580*, now identified as *PROSCOOP10* (Gully *et al.*,  
486 2019), is highly transcribed in the SAM during the first 9 days after germination, then the  
487 expression strongly decreased between 9 and 10 days, with a log<sub>2</sub> fold change of -4.54,  
488 ranking 30 out of 968 down-regulated genes between these two stages. *PROSCOOP10*  
489 expression remains at this low level at later stages of development. This expression profile is

490 intriguingly similar to that of *FLOWERING LOCUS (FLC)* another flowering regulator and  
491 opposite to *LEAFY* whose expression increase during the transition to flowering (Klepikova *et*  
492 *al.*, 2015). While the expression of *PROSCOOP10* in leaves seems rather constitutive, its  
493 strikingly different expression profile in the SAM could fit with the early flowering phenotype of  
494 the *proscoop10* mutants. Additionally, the transcriptomic profiles of *PROSCOOP10* in various  
495 mutants or experimental conditions always showed a negative correlation between the level of  
496 *PROSCOOP10* expression and the time span before flowering (**Table 1**). Indeed, studies have  
497 shown that *PROSCOOP10* is repressed in plants showing an early flowering phenotype such  
498 as in the *abi4vtc2* and *phyABCDE* mutants compared to their corresponding wild-type (Foyer  
499 *et al.*, 2012; Hu *et al.*, 2013). Furthermore, in mutants such as *vtc2*, *tcp4* and *ga1-3* which  
500 display a late flowering phenotype or no flowering at all, *PROSCOOP10* is induced (Blazquez  
501 *et al.*, 1998; Pavet *et al.*, 2005; Kubota *et al.*, 2017). In the *arf6-2/arf8-3* mutant, inflorescence  
502 stems elongate less than those of the wild-type and flowers arrest as infertile closed buds with  
503 short petal. In this mutant, *PROSCOOP10* is also highly expressed in comparison with the  
504 wild-type (Nagpal *et al.*, 2005). All these results suggest that *PROSCOOP10* interferes with  
505 the floral transition process, upstream of *SOC1* and *LEAFY*, to delay flowering. Then,  
506 *PROSCOOP10* could be another player of the meristem identity as a delayer of floral transition,  
507 the actual signalling cascade remaining unknown. A putative role in the maintenance of the  
508 vegetative state could also be suggested after the work published by Moon *et al.* in 2007, as  
509 *PROSCOOP10* was one of the two genes co-regulated with *PIF1*, itself also reported as  
510 optimizing the greening process. The fact that *PROSCOOP10* is rather constitutively  
511 expressed in the green parts of the plant could support this hypothesis, as well as its huge  
512 decrease of expression when the SAM acquires its floral identity (Klepikova *et al.*, 2015). The  
513 involvement of *PROSCOOP10* and the respective functions of both *SCOOP10#1* and  
514 *SCOOP10#2*, that we have identified, need further investigations to clarify their roles in these  
515 mechanisms and identify their target and downstream signalling cascade. Altogether, these  
516 data may link *PROSCOOP10* to the flowering-time control or the floral transition and illustrate  
517 the functional complexity of the *PROSCOOP* family.

518

519 **Table 1: Expression profile of the *PROSCOOP10* genes extracted from public data**

Condition	Phenotype	<i>PROSCOOP10</i> transcription	Reference
10 <sup>th</sup> vs 9 <sup>th</sup> day, in SAM wild-type	wild-type	Down-regulated	Klepikova <i>et al.</i> , 2015
<i>pif1-5</i> vs wild-type	early flowering	Down-regulated	Moon <i>et al.</i> , 2007 ; Wu <i>et al.</i> , 2018
<i>abi4vtc2</i> vs wild-type	early flowering	Down-regulated	Foyer <i>et al.</i> , 2012
<i>phyABCDE</i> vs wild-type	early flowering	Down-regulated	Hu <i>et al.</i> , 2013
brassinolide treatment on wild-type	early flowering	Down-regulated	Li <i>et al.</i> , 2010
MeJA treatment on wild-type	early flowering	Down-regulated	Pak <i>et al.</i> , 2009
35S:: <i>ARAF1</i> vs wild-type	late flowering	Up-regulated	Chavez <i>et al.</i> , 2008
<i>vtc2</i> vs wild-type	late flowering	Up-regulated	Pavet <i>et al.</i> , 2005
<i>tcp4</i> vs wild-type	late flowering	Up-regulated	Kubota <i>et al.</i> , 2017
<i>ga1-3</i> vs wild-type	no flowering	Up-regulated	Blazquez <i>et al.</i> , 1998
<i>arf6-2/arf8-3</i> vs wild-type	immature flowers	Up-regulated	Nagpal <i>et al.</i> , 2005

520

521

## 522 SUPPLEMENTARY DATA

523 **Supplementary Table S1:** Primer sets for genotyping

524 **Supplementary Table S2:** <sup>1</sup>H and <sup>13</sup>C NMR assignment of SCOOP10#2\* peptide 1 mM in 50  
525 mM phosphate buffer (10% D<sub>2</sub>O), pH 6.6, 278K

526 **Supplementary Table S3:** <sup>1</sup>H and <sup>13</sup>C NMR assignment of hydroxylated SCOOP10#2 peptide  
527 0.5 mM in 50 mM phosphate buffer (10% D<sub>2</sub>O), pH 6.6, 278 K

528 **Supplementary Table S4:** <sup>1</sup>H and <sup>13</sup>C NMR assignment of SCOOP10#2\* peptide 0.5 mM in  
529 DMSO, 298K

530 **Supplementary Table S5:** <sup>1</sup>H and <sup>13</sup>C NMR assignment of hydroxylated SCOOP10#2 peptide  
531 0.5 mM in DMSO, 298K

532 **Supplementary Table S6:** <sup>1</sup>H and <sup>13</sup>C NMR assignment of hydroxylated SCOOP10#1 peptide  
533 0.5 mM in 50 mM phosphate buffer (10% D<sub>2</sub>O), pH 6.6, 278K

534 **Supplementary Table S7:** <sup>1</sup>H and <sup>13</sup>C NMR assignment of hydroxylated SCOOP10#1 peptide  
535 0.5 mM in DMSO, 298K

536 **Supplementary Table S8:** Number of bolted inflorescences for Col-0 and *proscop10* mutants  
537 per day after germination and per repetition

538

539 **Supplementary Figure S1: Genotyping of *proscoop10* mutant lines**

540 (A) Position of the T-DNA insertion in the *proscoop10-1* mutant. (B) On the left, check of the  
541 T-DNA insertion by PCR on *PROSCOOP10* and comparison with PCR on *AtCOP1*, used as a  
542 PCR positive control, in DNA of Col-0 and *proscoop10-1* mutant. On the right, check of  
543 *PROSCOOP10* expression impairment in *proscoop10-1* mutant compared to Col-0 wild-type,  
544 with *AtCOP1* used at RT-PCR positive control. (C) Position of the two RNA guides targeting  
545 SCOOP10#1 and SCOOP10#2 regions in the *proscoop10-2* mutant. (D) Reference sequence  
546 of PROSCOOP10. In red, the start and stop codons; in orange, the primer used for PCR  
547 amplification and sequencing after cloning; highlighted in grey, the guides RNAg1 and RNAg2  
548 and in bold, the PAM1 and PAM2. (E) Sequencing revealed two different alleles in the therefore  
549 bi allelic *proscoop10-2* mutant. Alignments with the reference sequence shown for the first  
550 mutated allelic version a deletion of 237 bp between the two guides, in addition to nucleotide  
551 modifications in guides RNAg1 and RNAg2. This led to a deletion into SCOOP10#1 sequence  
552 and a frameshift generating a stop codon and eliminating the SCOOP10#2 sequence. For the  
553 second mutated allelic version, an important deletion of 448 bp has been generated between  
554 the two guides, leading to a break in the two sequences corresponding to SCOOP10#1 and  
555 SCOOP10#2 and a fusion of the remaining sequences. (F) Amino acid sequences of  
556 PROSCOOP10 in *proscoop10-2* bi allelic mutant after CRISPR/Cas9 edition. For (A) and (C)  
557 exons (CDS) and introns are represented by boxes and lines respectively. For (A), (C) and  
558 (F) purple: SCOOP10#1 region; blue: SCOOP10#2 region; green: signal peptide; red star: stop  
559 codon.

560 **Supplementary Figure S2: MS data related to SCOOP10#1 and SCOOP10#2 originating**  
561 **from PROSCOOP10 identified in rosette leaves apoplastic fluids**

562 (A-H) For each peptide, a representative MS/MS spectrum is shown. The positions of the  
563 hydroxyproline (O)/proline (P) residues are highlighted using the fragmentation data from the  
564 C-terminus of each peptide (y ions). The information describing the experimental procedure is  
565 available in Material and Methods.

566 **Supplementary Figure S3: NMR assignment and cis/trans isomerization of SCOOP10#2**  
567 **in DMSO.** (A) NMR assignment of SCOOP10#2 reported on 1H,1H-TOCSY spectrum (HN/H $\alpha$   
568 region). (B) 1H,1H-NOESY cross-peaks between H $\alpha$  protons of G6 and H $\alpha$  or H $\alpha$  protons of  
569 hydroxyproline in position 7 indicating the presence of both cis and trans conformation of the  
570 G6-P7 peptide bond, respectively.

571 **Supplementary Figure S4: MD simulations of SCOOP10#2 mutants.** (A) DSSP secondary  
572 structures calculated along the trajectories. (B) Contact maps of selected mutants.

573 **Supplementary Figure S5: Representative structures found in MD simulations for**  
574 **SCOOP10#2 and its mutants.** For each structure the tube (left) and ribbon (right) renderings  
575 are shown.

576 **Supplementary Figure S6: Structural behaviour of SCOOP10#1 in solution as monitored**  
577 **by NMR.** Chemical shifts deviations from random coil values of H $\alpha$  protons and of the  
578 difference between C $\alpha$  and C $\beta$  carbons suggest the absence of a well definite structure for  
579 SCOOP10#1. Deviations for glycine H $\alpha$  atoms were intentionally omitted.

580 **Supplementary Figure S7: Secondary structures and intramolecular interactions found**  
581 **in MD simulations of SCOOP10#1.** (A) DSSP secondary structures calculated along  
582 molecular dynamics (MD) simulation of hydroxylated SCOOP10#1 in solution. (B) Occurrence  
583 of intramolecular polar atom contacts (H-bonds and salt bridges) in SCOOP10#1 calculated  
584 along MD simulation trajectories. (C) Contact map.

585

## 586 **ACKNOWLEDGEMENTS**

587 The authors are thankful to INRAE, CNRS, Angers University, Paul Sabatier-Toulouse 3  
588 University, Angers Loire Métropole, French Region Pays de la Loire and Agence Nationale de  
589 la Recherche (ANR) to support their work. The authors thank Prof. Andreas Schaller  
590 (University of Hohenheim, Germany) and Prof. Cyril Zipfel (University of Zurich, Switzerland)  
591 for helpful discussions, Denis Hellal (Université Paris-Est Créteil, France) for help in the  
592 molecular dynamics simulations and Sophie Aligon (IRHS Angers, France) for plant care.

## 593 **AUTHOR CONTRIBUTIONS**

594 SA (project coordinator), J-PR and EJ designed and supervised the experiments. M-CG, EV  
595 and MA-A performed the mutant production, phenotyping, peptide assays, and RT-qPCR  
596 analysis. TB, MZ, EJ, HC and JC performed MS analysis of apoplastic fluids. CH-L, ND'A, FR-  
597 M and ER analysed peptide structure through RMN and molecular dynamics. M-CG, ND'A,  
598 ER, J-PR, EJ and SA wrote the manuscript and all authors read and approved the final version.

## 599 **CONFLICT OF INTEREST**

600 The authors declare no competing interest.

## 601 **FUNDINGS**

602 This research was funded by ANR (ANR-20-CE20-0025), Angers University and INRAE, and  
603 conducted in the framework of the regional program “*Objectif Végétal*, Research, Education  
604 and Innovation in Pays de la Loire”, supported by the French Region Pays de la Loire, Angers  
605 Loire Métropole and the European Regional Development Fund. Claudia Herrera-León’s PhD  
606 scholarship was funded by the National Council for Science and Technology (CONACYT).

## 607 **DATA AVAILABILITY**

608 All data supporting the findings of this study are available within the paper and within its  
609 supplementary materials published online. Biological materials are available from the  
610 corresponding authors upon request.

## 611 **REFERENCES**

612 Abraham MJ, Murtola T, Schulz R, Páll S, Smith JC, Hess B, *et al.* 2015. GROMACS: High  
613 performance molecular simulations through multi-level parallelism from laptops to  
614 supercomputers. *SoftwareX* 1, 19–25.

- 615 Amano Y, Tsubouchi H, Shinohara H, Ogawa M, Matsubayashi Y. 2007. Tyrosine-sulfated  
616 glycopeptide involved in cellular proliferation and expansion in Arabidopsis. Proceedings of the  
617 National Academy of Sciences USA 104, 18333-18338.
- 618 Araya T, von Wirén N, Takahashi H. 2014. CLE peptides regulate lateral root development in  
619 response to nitrogen nutritional status of plants. Plant Signaling and Behaviour 9, e29302.
- 620 Balliau T, Blein-Nicolas M, Zivy M. 2018. Evaluation of optimized tube-gel methods of sample  
621 preparation for large-scale plant proteomics. Proteomes 6, 6.
- 622 Blázquez MA, Green R, Nilsson O, Sussman MR, Weigel D. 1998. Gibberellins promote  
623 flowering of Arabidopsis by activating the LEAFY promoter. The Plant Cell 10, 791-800.
- 624 Boudart G, Jamet E, Rossignol M, Lafitte C, Borderies G, Jauneau A, *et al.* 2005. Cell wall  
625 proteins in apoplastic fluids of *Arabidopsis thaliana* rosettes: identification by mass  
626 spectrometry and bioinformatics. Proteomics 5, 212-221.
- 627 Canut H, Albenne C, Jamet E. 2016. Post-translational modifications of plant cell wall proteins  
628 and peptides: a survey from a proteomics point of view. Biochimica et Biophysica Acta (BBA)-  
629 Proteins and Proteomics 1864, 983-990.
- 630 Casamitjana-Martinez E, Hofhuis HF, Xu J, Liu CM, Heidstra R, Scheres B. 2003. Root specific  
631 CLE19 overexpression and the sol1/2 suppressors implicate a CLV-like pathway in the control  
632 of Arabidopsis root meristem maintenance. Current Biology 13, 1435–1441
- 633 Charrier A, Vergne E, Dousset N, Richer A, Petiteau A, Chevreau E. 2019. Efficient targeted  
634 mutagenesis in apple and first-time edition of pear using the CRISPR-Cas9 System. Frontiers  
635 in Plant Science 6,10-40.
- 636 DeLano WL. 2002. Pymol: An open-source molecular graphics tool. CCP4 Newsletter on  
637 protein crystallography 40, 82–92.
- 638 Dorman DE, Bovey FA. 1973. Carbon-13 magnetic resonance spectroscopy, the spectrum of  
639 proline in oligopeptides. Chemischer Informationsdienst 38, 2379-2383.
- 640 Duruflé H, Hervé V, Balliau T, Zivy M, Dunand C, Jamet E. 2017 Proline hydroxylation in cell  
641 wall proteins: is it yet possible to define rules? Frontiers in Plant Science 8, 1802
- 642 Duruflé H, Ranocha P, Balliau T, Dunand C, Jamet E. 2019. Transcriptomic and cell wall  
643 proteomic datasets of rosettes and floral stems from five *Arabidopsis thaliana* ecotypes grown  
644 at optimal or sub-optimal temperature. Data in Brief 27, 104581.

- 645 Gaggelli E, D'Amelio N, Gaggelli N, Valensin G. 2001. Metal ion effects on the cis/trans  
646 isomerization equilibrium of proline in short-chain peptides: a solution NMR study.  
647 ChemBioChem 2, 524–529.
- 648 Gagnot S, Tamby JP, Martin-Magniette ML, Bitton F, Taconnat L, Balzergue S, *et al.* 2007.  
649 CATdb: a public access to Arabidopsis transcriptome data from the URGV-CATMA platform.  
650 Nucleic Acids Research, 36, 986-990.
- 651 Guillou MC, Vergne E, Aligon S, Pelletier S, Simonneau F, Rolland A, Chabout S, Mouille G,  
652 Gully K, Grappin P, Montrichard F, Aubourg S, Renou JP. 2022. SCOOP12 peptide acts on  
653 ROS homeostasis to modulate cell division and elongation in Arabidopsis primary root. Journal  
654 of Experimental Botany, doi: 10.1093/jxb/erac240.
- 655 Gully K, Pelletier S, Guillou MC, Ferrand M, Aligon S, Pokotylo I, Perrin A, Vergne E, Fagard  
656 M, Ruelland E, Grappin P, Bucher E, Renou JP, Aubourg S. 2019. The SCOOP12 peptide  
657 regulates defense response and root elongation in *Arabidopsis thaliana*. Journal of  
658 Experimental Botany 70, 1349-1365.
- 659 Hou S, Liu D, Huang S, Luo D, Liu Z, Wang P, Mu R, Han Z, Chai J, Shan L, He P PH. 2021.  
660 Immune elicitation by sensing the conserved signature from phyto cytokines and microbes via  
661 the Arabidopsis MIK2 receptor. Nature Communications 12, 5494.
- 662 Hu W, Franklin KA, Sharrock RA, Jones MA, Harmer SL, Lagarias JC. 2013. Unanticipated  
663 regulatory roles for Arabidopsis phytochromes revealed by null mutant analysis. Proceedings  
664 of the National Academy of Sciences USA 110, 1542-1547.
- 665 Humphrey W, Dalke A, Schulten K. 1996. VMD: Visual molecular dynamics. Journal of  
666 Molecular Graphics 14, 33–38.
- 667 Janert PK. 2010. Gnuplot in Action: Understanding Data with Graphs. Simon and Schuster.
- 668 Kerchev PI, Pellny TK, Vivancos PD, Kiddle G, Hedden P, Driscoll S, *et al.* 2011. The  
669 transcription factor ABI4 is required for the ascorbic acid–dependent regulation of growth and  
670 regulation of jasmonate-dependent defense signaling pathways in Arabidopsis. The Plant Cell  
671 23, 3319-3334.
- 672 Klepikova AV, Logacheva MD, Dmitriev SE, Penin AA. 2015. RNA-seq analysis of an apical  
673 meristem time series reveals a critical point in *Arabidopsis thaliana* flower initiation. BMC  
674 Genomics 16, 466.
- 675 Krieger E, Vriend G. 2014. YASARA View - molecular graphics for all devices - from  
676 smartphones to workstations. Bioinformatics 30, 2981–2982.

- 677 Kubota A, Ito S, Shim JS, Johnson RS, Song YH, Breton G, Goralogia GS, Kwon MS, Laboy  
678 Cintrón D, Koyama T, Ohme-Takagi M, Pruneda-Paz JL, Kay SA, MacCoss MJ, Imaizumi T.  
679 2017. TCP4-dependent induction of CONSTANS transcription requires GIGANTEA in  
680 photoperiodic flowering in Arabidopsis. *PLoS Genet.* 13, e1006856.
- 681 Langella O, Valot B, Balliau T, Blein-Nicolas M, Bonhomme L, Zivy M. 2017. X!  
682 TandemPipeline: a tool to manage sequence redundancy for protein inference and  
683 phosphosite identification. *Journal of Proteome Research* 16, 494-503.
- 684 Lee W, Tonelli M, Markley JL. 2015. NMRFAM-SPARKY: enhanced software for biomolecular  
685 NMR spectroscopy. *Bioinformatics* 31, 1325–1327.
- 686 Lee W, Yu W, Kim S, Chang I, Lee W, Markley JL. 2012. PACSY, a relational database  
687 management system for protein structure and chemical shift analysis. *Journal of Biomolecular*  
688 *NMR* 54, 169–179.
- 689 Lemkul J. 2019. From proteins to perturbed Hamiltonians: A suite of tutorials for the  
690 GROMACS-2018 molecular simulation package [Article v1.0]. *Living Journal of Computational*  
691 *Molecular Science* 1, 5068.
- 692 Li J, Li Y, Chen S, An L. 2010. Involvement of brassinosteroid signals in the floral-induction  
693 network of Arabidopsis. *Journal of Experimental Botany* 61, 4221-4230.
- 694 Lindorff-Larsen K, Piana S, Palmo K, Maragakis P, Klepeis JL, Dror RO, *et al.* 2010. Improved  
695 side-chain torsion potentials for the Amber ff99SB protein force field. *Proteins: Structure,*  
696 *Function, and Bioinformatics* 78, 1950–1958.
- 697 Matsubayashi Y. 2011. Post-translational modifications in secreted peptide hormones in  
698 plants. *Plant and Cell Physiology* 52, 5-13.
- 699 Moon J, Zhu L, Shen H, Huq E. 2008. PIF1 directly and indirectly regulates chlorophyll  
700 biosynthesis to optimize the greening process in Arabidopsis. *Proceedings of the National*  
701 *Academy of Sciences USA* 105, 9433-9438.
- 702 Moon J, Zhu L, Shen H, Huq E. 2008. PIF1 directly and indirectly regulates chlorophyll  
703 biosynthesis to optimize the greening process in Arabidopsis. *Proceedings of the National*  
704 *Academy of Sciences USA* 105, 9433-9438.
- 705 Murphy E, Smith S, De Smet I. 2012. Small signaling peptides in Arabidopsis development:  
706 how cells communicate over a short distance. *The Plant Cell* 24, 3198-3217.

- 707 Nielsen JT, Mulder FAA. 2018. POTENCI: prediction of temperature, neighbor and pH-  
708 corrected chemical shifts for intrinsically disordered proteins. *Journal of Biomolecular NMR* 70,  
709 141–165.
- 710 Ohyama K, Ogawa M, Matsubayashi Y. 2008. Identification of a biologically active, small,  
711 secreted peptide in *Arabidopsis* by in silico gene screening, followed by LC-MS-based  
712 structure analysis. *The Plant Journal* 55, 152-60.
- 713 Parcy F. 2005. Flowering: a time for integration. *The International Journal of Developmental*  
714 *Biology* 49, 585–593.
- 715 Pauwels L, De Clercq R, Goossens J, Iñigo S, Williams C, Ron M *et al.* 2018. A dual sgRNA  
716 approach for functional genomics in *Arabidopsis thaliana*. *G3: Genes, Genomes, Genetics* 8,  
717 2603-2615.
- 718 Pavet V, Olmos E, Kiddle G, Mowla S, Kumar S, Antoniw J, Alvarez ME, Foyer CH. 2005.  
719 Ascorbic acid deficiency activates cell death and disease resistance responses in *Arabidopsis*.  
720 *Plant Physiology* 139, 1291–1303.
- 721 Pettersen EF, Goddard TD, Huang CC, Couch GS, Greenblatt DM, Meng EC, *et al.* 2004.  
722 UCSF Chimera-A visualization system for exploratory research and analysis. *Journal of*  
723 *Computational Chemistry* 25, 1605–1612.
- 724 Pokotylo I, Hellal D, Bouceba T, Hernandez-Martinez M, Kravets V, Leitao L, *et al.* 2020.  
725 Deciphering the binding of salicylic acid to *Arabidopsis thaliana* chloroplastic GAPDH-A1.  
726 *International Journal of Molecular Sciences* 21, 4678.
- 727 Pucheta-Martínez E, Saladino G, Morando MA, Martínez-Torrecedrada J, Lelli M, Sutto L, *et*  
728 *al.* 2016. An allosteric cross-talk between the activation loop and the ATP binding site regulates  
729 the activation of Src kinase. *Scientific Reports* 6, 1-7.
- 730 Ramos-Martín F, Herrera-León C, Antonietti V, Sonnet P, Sarazin C, D'Amelio N. 2020.  
731 Antimicrobial peptide k11 selectively recognizes bacterial biomimetic membranes and acts by  
732 twisting their bilayers. *Pharmaceuticals* 14, 1.
- 733 Rhodes J, Yang H, Moussu S, Boutrot F, Santiago J, Zipfel C. 2021. Perception of a divergent  
734 family of phytocytokines by the *Arabidopsis* receptor kinase MIK2. *Nature Communications* 12,  
735 705.
- 736 Roberts I, Smith S, De Rybel B, Van Den Broeke J, Smet W, De Cokere S, Mispelaere M, De  
737 Smet I, Beeckman T. 2013. The CEP family in land plants: evolutionary analyses, expression  
738 studies, and role in *Arabidopsis* shoot development. *Journal of Experimental Botany* 64, 5371-  
739 5381.

- 740 Roux F, Touzet P, Cuguen J, Le Corre V. 2006. How to be early flowering: an evolutionary  
741 perspective. *Trends in Plant Science* 11, 375-381.
- 742 Royek S, Bayer M, Pfannstiel J, Pleiss J, Ingram G, Stintzi A, Schaller A. 2022. Processing of  
743 a plant peptide hormone precursor facilitated by posttranslational tyrosine sulfation.  
744 *Proceedings of the National Academy of Sciences USA* 119, e2201195119.
- 745 San Clemente H, Jamet E. 2015. WallProtDB, a database resource for plant cell wall  
746 proteomics. *Plant Methods* 11, 2.
- 747 San Clemente H, Kolkas H, Canut H, Jamet E. 2022. Plant cell wall proteomes: the core of  
748 conserved protein families and the case of non-canonical proteins. *International Journal of*  
749 *Molecular Sciences* 22, 4273.
- 750 Schaller A, Stintzi A, Graff L. 2012. Subtilases—versatile tools for protein turnover, plant  
751 development, and interactions with the environment. *Physiologia Plantarum* 145, 52-66.
- 752 Schardon K, Hohl M, Graff L, Schulze W, Pfannstiel J, Stintzi A, Schaller A. 2016. Precursor  
753 processing for plant peptide hormone maturation by subtilisin-like serine proteinases. *Science*  
754 354, 1594-1597.
- 755 Sekhar A, Velyvis A, Zoltsman G, Rosenzweig R, Bouvignies G, Kay LE. 2018. Conserved  
756 conformational selection mechanism of Hsp70 chaperone-substrate interactions. *Elife* 7,  
757 e32764.
- 758 Simpson GG. and Dean C. 2002 Arabidopsis, the Rosetta stone of flowering time? *Science*,  
759 296, 285–289.
- 760 Shinohara H, Matsubayashi Y. 2010. Arabinosylated glycopeptide hormones: new insights into  
761 CLAVATA3 structure. *Current Opinion in Plant Biology* 13, 515-519.
- 762 Shinohara H, Matsubayashi Y. 2013. Chemical synthesis of Arabidopsis CLV3 glycopeptide  
763 reveals the impact of hydroxyproline arabinosylation on peptide conformation and activity.  
764 *Plant and Cell Physiology* 54, 369-374.
- 765 Showalter AM, Keppler B, Lichtenberg J, Gu D, Welch LR. 2010. A bioinformatics approach to  
766 the identification, classification, and analysis of hydroxyproline-rich glycoproteins. *Plant*  
767 *Physiology* 153, 485-513.
- 768 Siemion IZ, Wieland T, Pook K-H. 1975. Influence of the distance of the proline carbonyl from  
769 the  $\beta$  and  $\gamma$  carbon on the  $^{13}\text{C}$  chemical shifts. *Angewandte Chemie International Edition in*  
770 *English* 14, 702–703.

- 771 Smith DJ, Klauda JB, Sodt AJ. 2019. Simulation Best Practices for Lipid Membranes [Article  
772 v1.0]. *Living Journal of Computational Molecular Science* 1, 5966.
- 773 Stintzi A, Schaller A. 2022. Biogenesis of post-translationally modified peptide signals for plant  
774 reproductive development. *Current Opinion in Plant Biology* 69, 102274.
- 775 Tamaki T, Betsuyaku S, Fujiwara M, Fukao Y, Fukuda H, Sawa S. 2013. SUPPRESSOR OF  
776 LLP 1 1-mediated C-terminal processing is critical for CLE 19 peptide activity. *The Plant*  
777 *Journal* 76, 970-981.
- 778 Takahashi F, Suzuki T, Osakabe Y, Betsuyaku S, Kondo Y, Dohmae N, Fukuda H, Yamaguchi-  
779 Shinozaki K, Shinozaki K. 2018. A small peptide modulates stomatal control via abscisic acid  
780 in long-distance signalling. *Nature* 556, 235-238.
- 781 Tan L, Leykam JF, Kieliszewski MJ. 2003. Glycosylation motifs that direct arabinogalactan  
782 addition to arabinogalactan-proteins. *Plant Physiology* 1323, 1362-1369.
- 783 Tavormina P, De Coninck B, Nikonorova N, De Smet I, Cammue BPA. 2015. The Plant  
784 Peptidome: An Expanding Repertoire of Structural Features and Biological Functions. *The*  
785 *Plant Cell* 27, 2095-2118.
- 786 Vandesompele J, De Preter K, Pattyn F, Poppe B, Van Roy N, De Paepe A, Speleman F.  
787 2002. Accurate normalization of real-time quantitative RT-PCR data by geometric averaging  
788 of multiple internal control genes. *Genome Biology* 3, 1-12.
- 789 Vie AK, Najafi J, Liu B, Winge P, Butenko MA, Hornslien KS, Kumpf R, Aalen RB, Bones AM,  
790 Brembu T. 2015. The IDA/IDA-LIKE and PIP/PIP-LIKE gene families in Arabidopsis:  
791 phylogenetic relationship, expression patterns, and transcriptional effect of the PIPL3 peptide.  
792 *Journal of Experimental Botany* 66, 5351–5365.
- 793 Wang Y, Jardetzky O. 2002. Probability-based protein secondary structure identification using  
794 combined NMR chemical-shift data. *Protein Science* 11, 852–861.
- 795 Wedemeyer WJ, Welker E, Scheraga HA. 2002. Proline cis-trans isomerization and protein  
796 folding. *Biochemistry* 41,14637–14644.
- 797 Wishart DS, Bigam CG, Yao J, Abildgaard F, Dyson HJ, Oldfield E, *et al.* 1995. <sup>1</sup>H, <sup>13</sup>C and  
798 <sup>15</sup>N chemical shift referencing in biomolecular NMR. *Journal of Biomolecular NMR* 6, 135–  
799 140.
- 800 Wishart DS, Sykes BD, Richards FM. 1992. The chemical shift index: a fast and simple method  
801 for the assignment of protein secondary structure through NMR spectroscopy. *Biochemistry*  
802 31, 1647–1651.

803 Wishart DS, Sykes BD. 1994. The <sup>13</sup>C chemical-shift index: a simple method for the  
804 identification of protein secondary structure using <sup>13</sup>C chemical-shift data. *Journal of*  
805 *Biomolecular NMR* 4, 171-180.

806 Wishart DS. 2011. Interpreting protein chemical shift data. *Progress in Nuclear Magnetic*  
807 *Resonance Spectroscopy* 58, 62-87.

808 Wu M, Liu D, Abdul W, Upreti S, Liu Y, Song G, *et al.* 2018. PIL5 represses floral transition in  
809 *Arabidopsis* under long day conditions. *Biochemical and Biophysical Research*  
810 *Communications* 499, 513-518.

811 Yang J, Yan R, Roy A, Xu D, Poisson J, Zhang Y. 2015. The I-TASSER Suite: protein structure  
812 and function prediction. *Nature Methods* 12, 7–8.

813 Yu Z, Xu Y, Zhu L, Zhang L., Liu L, Zhang D, *et al.* 2020. The Brassicaceae-specific secreted  
814 peptides, STMPs, function in plant growth and pathogen defense. *Journal of Integrative Plant*  
815 *Biology* 62, 403-420.

816 Zimmermann P, Hirsch-Hoffmann M, Hennig L, Gruissem W. 2004. GENEVESTIGATOR.  
817 *Arabidopsis* microarray database and analysis toolbox. *Plant Physiology* 136, 2621-2632.

818 Zhang J, Zhao J, Yang Y, Bao Q, Li Y, Wang H, Hou S. 2022. EWR1 as a SCOOP peptide  
819 activates MIK2-dependent immunity in *Arabidopsis*. *Journal of Plant Interactions* 17, 562-568.

820 Zhang X, Henriques R, Lin SS, Niu QW, Chua NH. 2006. *Agrobacterium*-mediated  
821 transformation of *Arabidopsis thaliana* using the floral dip method. *Nature Protocols* 1, 641-  
822 646.

823

## 824 **FIGURE LEGEND**

### 825 **Figure 1: Identification of two SCOOP10 peptides by MS.**

826 (A) Sequence of the prepropeptide PROSCOOP10. The predicted signal peptide is in green, the mature  
827 SCOOP10#1 in purple and the mature SCOOP10#2 in blue. The tryptic cut sites (arginine (R) and lysine  
828 (K)) are indicated with yellow discs. The proline residues which were found to be hydroxylated are in  
829 black and underlined (P). The conserved serine residues are in bold. (B) Description of the different  
830 peptides covering the SCOOP10#1 and SCOOP10#2 amino acid sequences. The positions of P  
831 hydroxylation are indicated with O which stands for hydroxyproline. Stars indicate that the peptide has  
832 been identified after tryptic digestion. The frequency of observations of each peptide is indicated as well  
833 as the percentage of occurrences. (C) A focus on SCOOP10#2 to show the number of observations and  
834 the frequency of hydroxylation events at each P position.

835 **Figure 2: Structural behaviour of SCOOP10#2 and SCOOP10#2\* in solution**

836 (A)  $^1\text{H}$ ,  $^{13}\text{C}$ -HSQC spectrum assignment of non-hydroxylated SCOOP10#2\* (blue) and hydroxylated  
837 SCOOP10#2 (red) 0.5 mM in 50 mM phosphate buffer at pH 6.6 and 278 K. (B) Chemical shifts  
838 deviations from random coil values of H $\alpha$  protons and of the difference between C $\alpha$  and C $\beta$  carbons  
839 suggest the absence of a well definite structure for SCOOP10#2. Deviations for glycine H $\alpha$  atoms were  
840 intentionally omitted.

841 **Figure 3: Secondary structures and intramolecular interactions found in MD simulations**  
842 **of SCOOP10#2.**

843 (A) DSSP secondary structures calculated along molecular dynamics (MD) simulation of hydroxylated  
844 SCOOP10#2 in solution; (B) Occurrence of intramolecular polar atom contacts (H-bonds and salt  
845 bridges) in SCOOP10#2 calculated along MD simulation trajectories; (C, D) Schematic representations  
846 of SCOOP10#2 shown as a 'tube' coloured from blue (N-terminus) to red (C-terminus). Side-chains are  
847 shown as sticks with the following color code: positively charged (blue) and non-polar (light gray). The  
848 structures were created with PyMol (DeLano *et al.*, 2002). Key intramolecular interactions are indicated  
849 by two short parallel dashes.

850 **Figure 4: Effect of SCOOP10 peptides on seedling growth and on ROS production**

851 (A) Seedling growth inhibition evaluation by fresh mass measuring after 1  $\mu\text{M}$  elicitor or control  
852 treatment. (B)  $\text{H}_2\text{O}_2$  production after 1  $\mu\text{M}$  elicitor treatment or control treatment, measured with a  
853 luminol-based assay using leaf discs from 4-week-old plants of the indicated genotypes. Data  
854 represented are means of three independent replicates of over times RLU (relative luminescence units)  
855 ( $n=3$ ,  $\pm\text{SEM}$ ). For (A) and (B), SCOOP10#1 and SCOOP10#2 correspond to the proline hydroxylated  
856 peptides and prolines are not hydroxylated for the SCOOP10#2\*peptide.

857 **Figure 5: *proscop10* early flowering phenotype.**

858 (A) Bolted inflorescence of the *proscop10* mutant lines, the 22<sup>nd</sup> day after germination, indicated by the  
859 white arrows. (B) Delay of stem development between mutants and WT due to the early flowering of the  
860 *proscop10* lines, at the 27<sup>th</sup> day after germination. Scale bar = 1cm for (A) and (B). (C) Average of day  
861 to bolting for each genotype. (D) Kinetics represent the number of bolted inflorescences in %, starting  
862 from day 20 to day 30 after germination. ( $n=25$ ). (E) Average of the number of rosette leaves at the  
863 flowering time for each genotype. For (C) and (E) ANOVA and Tukey test allowed to define significantly  
864 two different groups labelled a and b.

865 **Figure 6: Impact of *PROSCOOP10* mutation on transcription of genes involved in floral**  
866 **regulation**

867 Relative expression of *SOC1*, *LEAFY* and *GA3OX-1* genes was measured by RT-qPCR after 7 days (in  
868 grey) and 11 days (in black) in the two *proscop10* mutant lines compared to Col-0 at 7 days. Values  
869 represent mean ratios  $\pm$  SEM of three independent biological replicates. Asterisks denote statistical  
870 differences of gene expression levels between *proscop10* mutants and Col-0 : \* $P < 0.05$ , \*\* $P < 0.01$   
871 (ratio paired t-test).

872 **FIGURES**

873

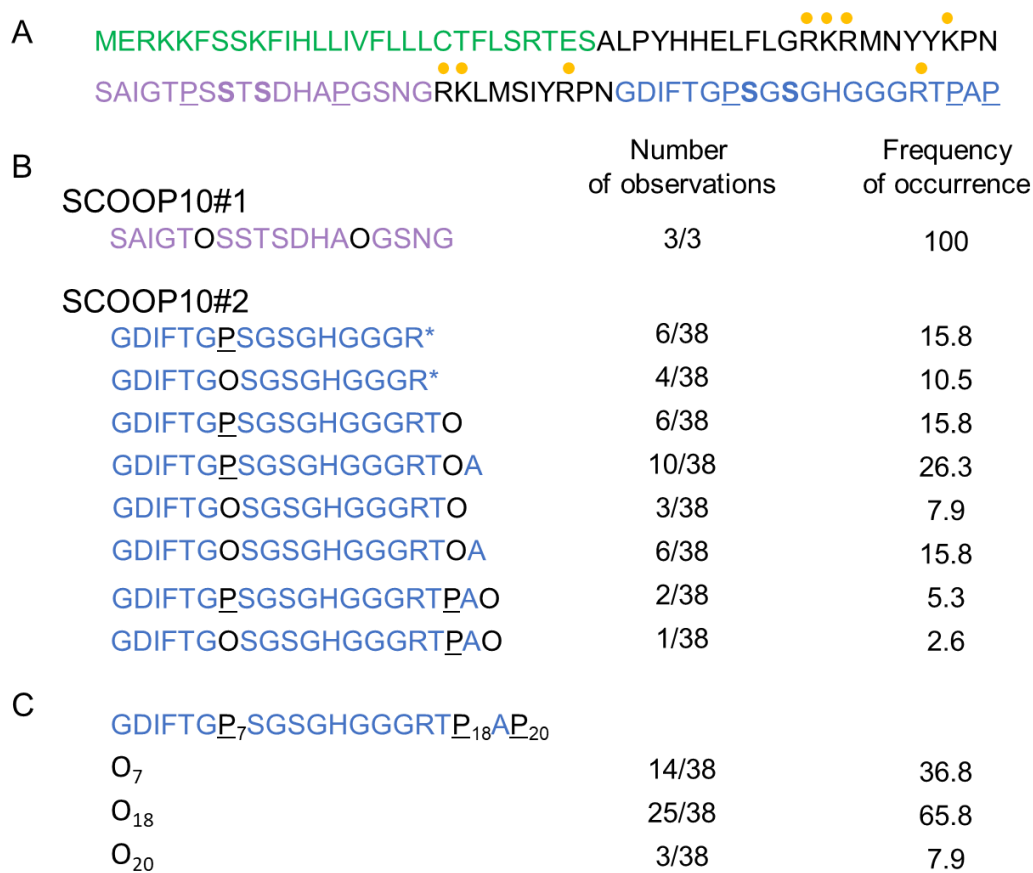


**Figure 4: Identification of two SCOOP10 peptides by MS.**

(A) Sequence of the prepropeptide PROSCOOP10. The predicted signal peptide is in green, the mature SCOOP10#1 in purple and the mature SCOOP10#2 in blue. The tryptic cut sites (arginine (R) and lysine (K)) are indicated with yellow discs. The proline residues which were found to be hydroxylated are in black and underlined (P). The conserved serine residues are in bold. (B) Description of the different peptides covering the SCOOP10#1 and SCOOP10#2 amino acid sequences. The positions of P hydroxylation are indicated with O which stands for hydroxyproline. Stars indicate that the peptide has been identified after tryptic digestion. The frequency of observations of each peptide is indicated as well as the percentage of occurrences. (C) A focus on SCOOP10#2 to show the number of observations and the frequency of hydroxylation events at each P position.

874

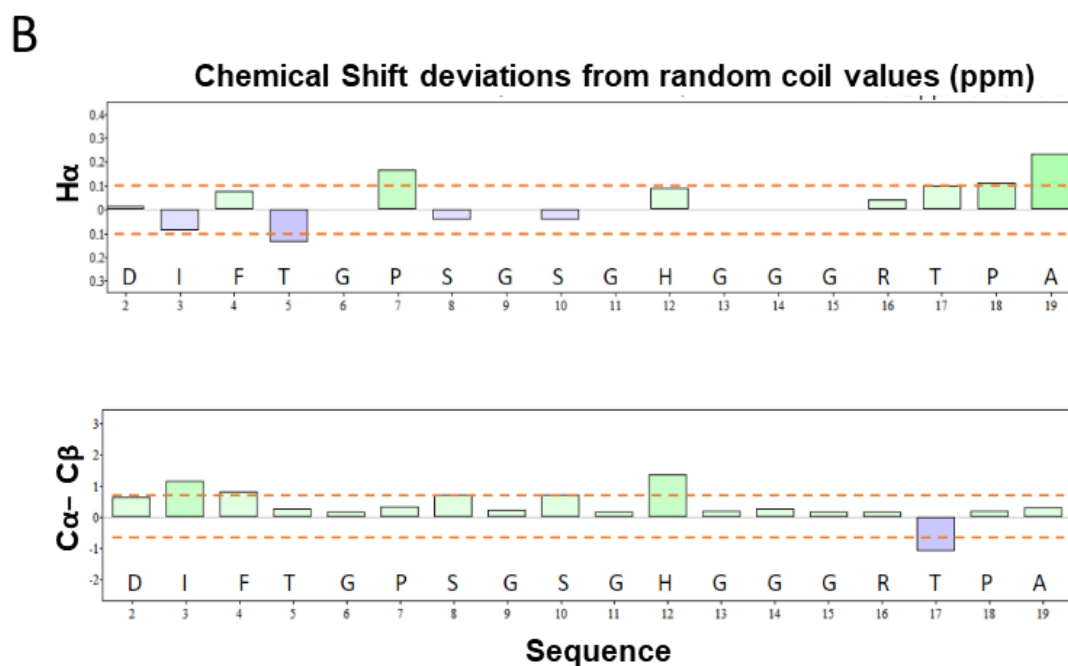
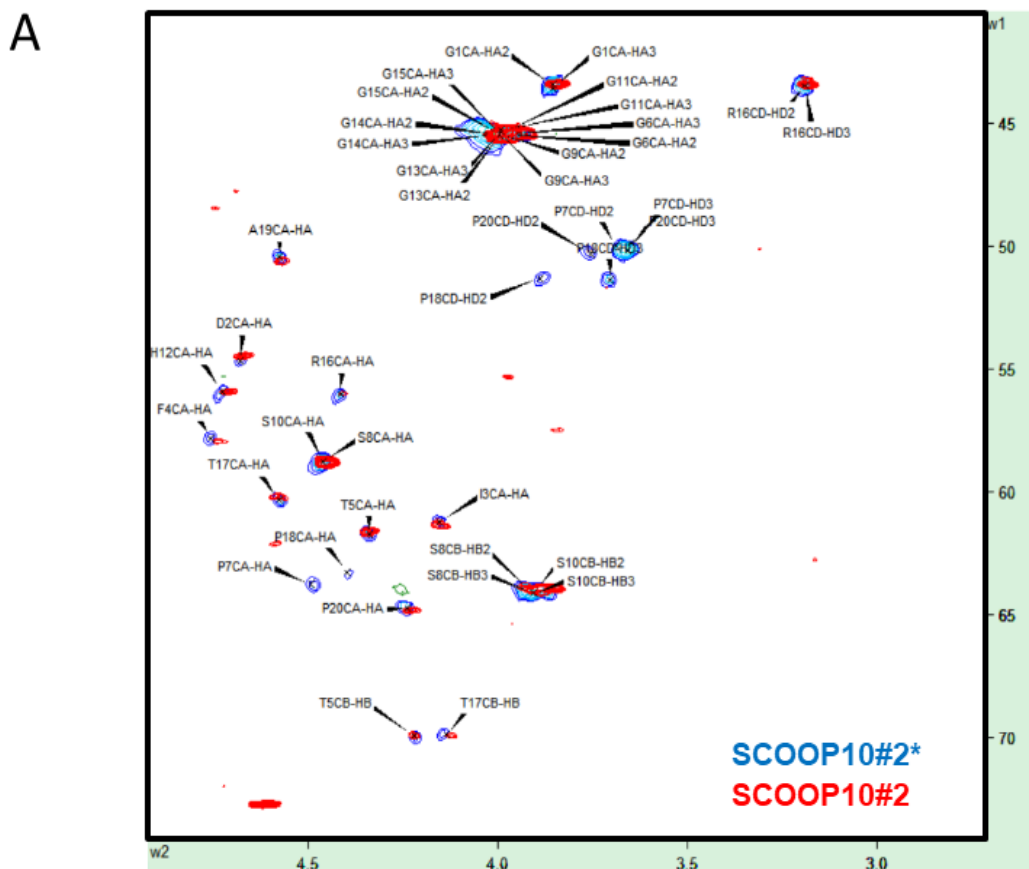


**Figure 5: Structural behaviour of SCOOP10#2 and SCOOP10#2\* in solution**

(A)  $^1\text{H}$ ,  $^{13}\text{C}$ -HSQC spectrum assignment of non-hydroxylated SCOOP10#2\* (blue) and hydroxylated SCOOP10#2 (red) 0.5 mM in 50 mM phosphate buffer at pH 6.6 and 278 K. (B) Chemical shifts deviations from random coil values of H $\alpha$  protons and of the difference between C $\alpha$  and C $\beta$  carbons suggest the absence of a well definite structure for SCOOP10#2. Deviations for glycine H $\alpha$  atoms were intentionally omitted.

875

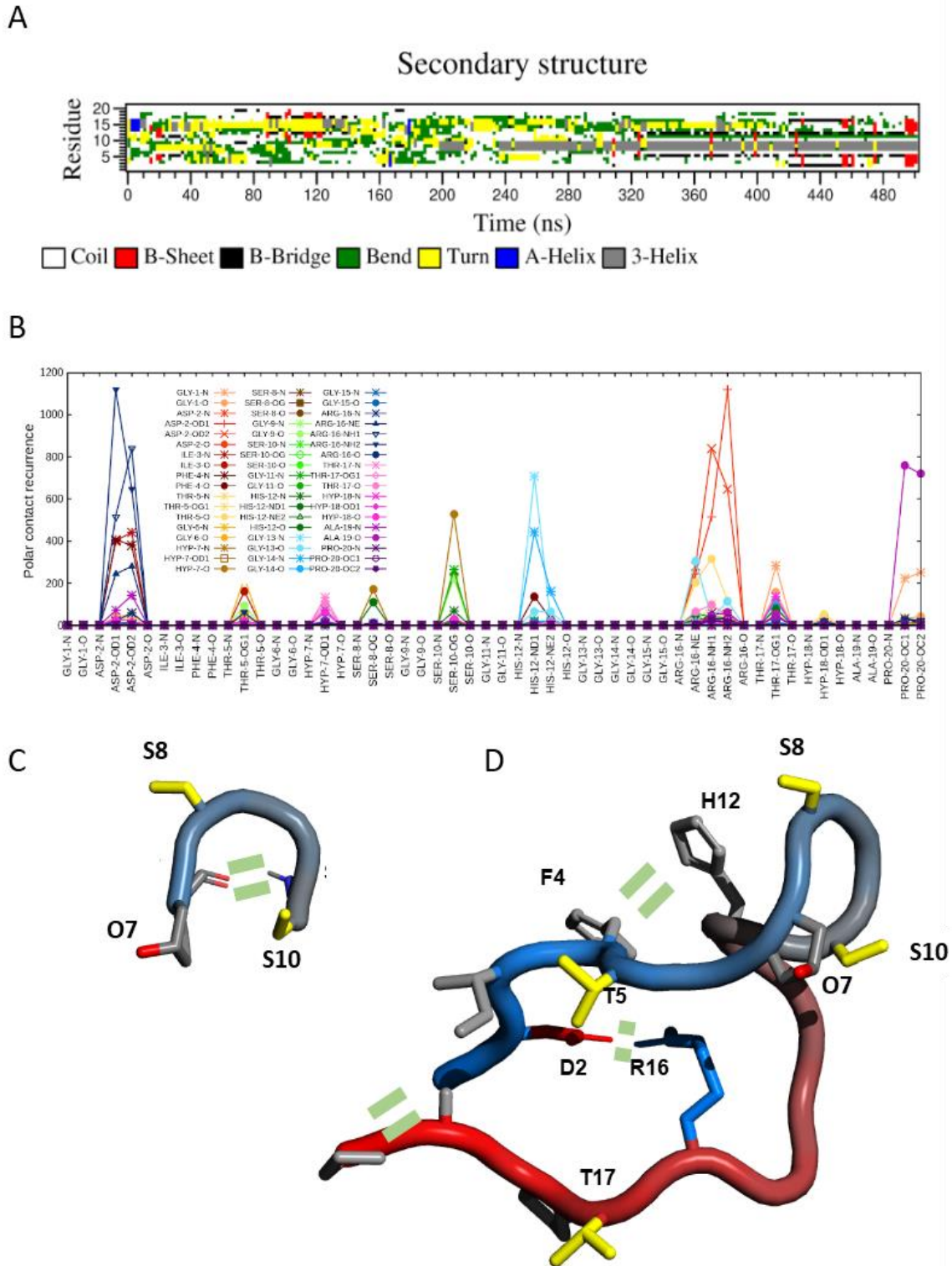


**Figure 6: Secondary structures and intramolecular interactions found in MD simulations of SCOOP10#2.**

(A) DSSP secondary structures calculated along molecular dynamics (MD) simulation of hydroxylated SCOOP10#2 in solution; (B) Occurrence of intramolecular polar atom contacts (H-bonds and salt bridges) in SCOOP10#2 calculated along MD simulation trajectories; (C, D) Schematic representations of SCOOP10#2 shown as a ‘tube’ coloured from blue (N-terminus) to red (C-terminus). Side-chains are shown as sticks with the following color code: positively charged (blue) and non-polar (light gray). The structures were created with PyMol (DeLano *et al.*, 2002). Key intramolecular interactions are indicated by two short parallel dashes.

876

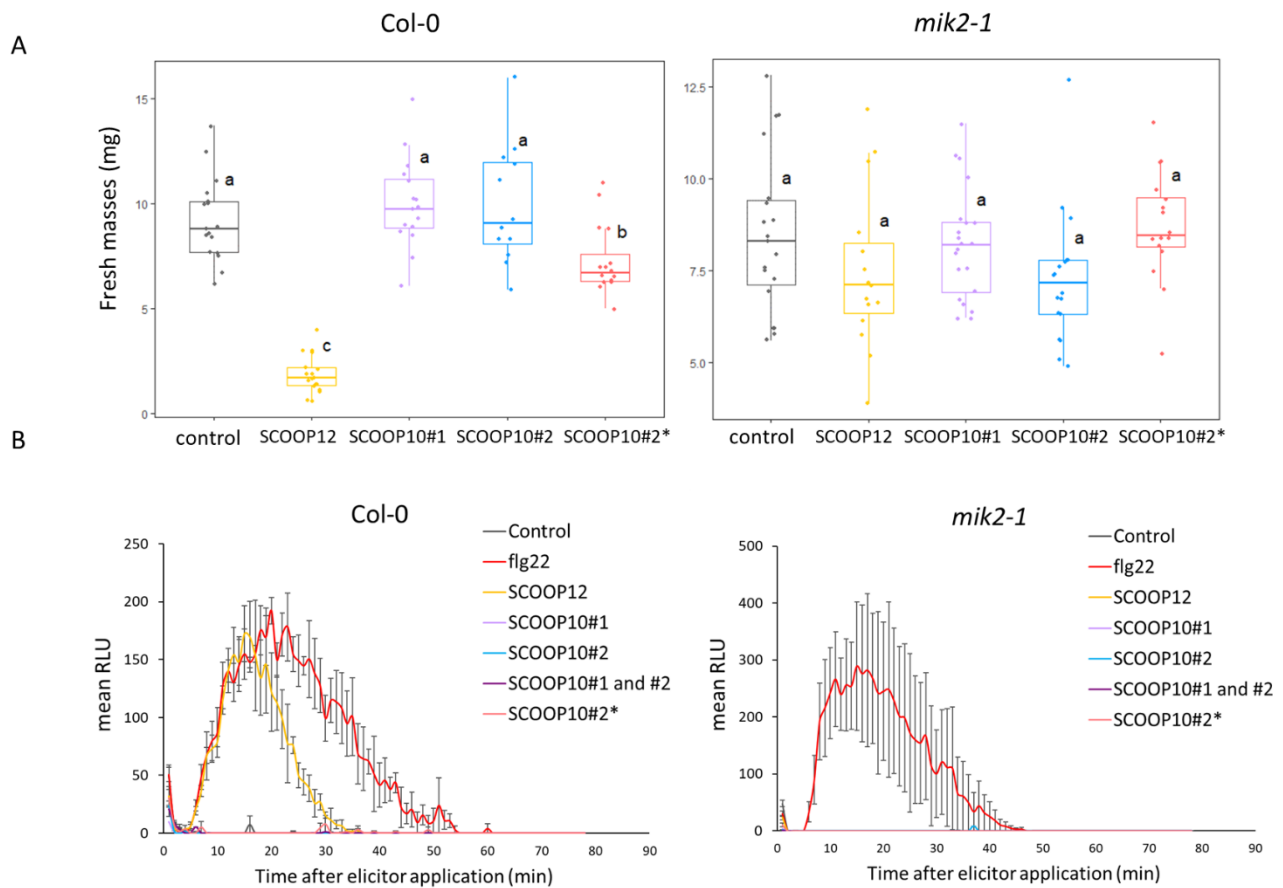


**Figure 4: Effect of SCOOP10 peptides on seedling growth and on ROS production**

(A) Seedling growth inhibition evaluation by fresh mass measuring after 1  $\mu$ M elicitor or control treatment.

(B)  $H_2O_2$  production after 1  $\mu$ M elicitor treatment or control treatment, measured with a luminol-based assay using leaf discs from 4-week-old plants of the indicated genotypes. Data represented are means of three independent replicates of over times RLU (relative luminescence units) ( $n = 3$ ,  $\pm$ SEM). For (A) and (B), SCOOP10#1 and SCOOP10#2 correspond to the proline hydroxylated peptides and prolines are not hydroxylated for the SCOOP10#2\*peptide.

877

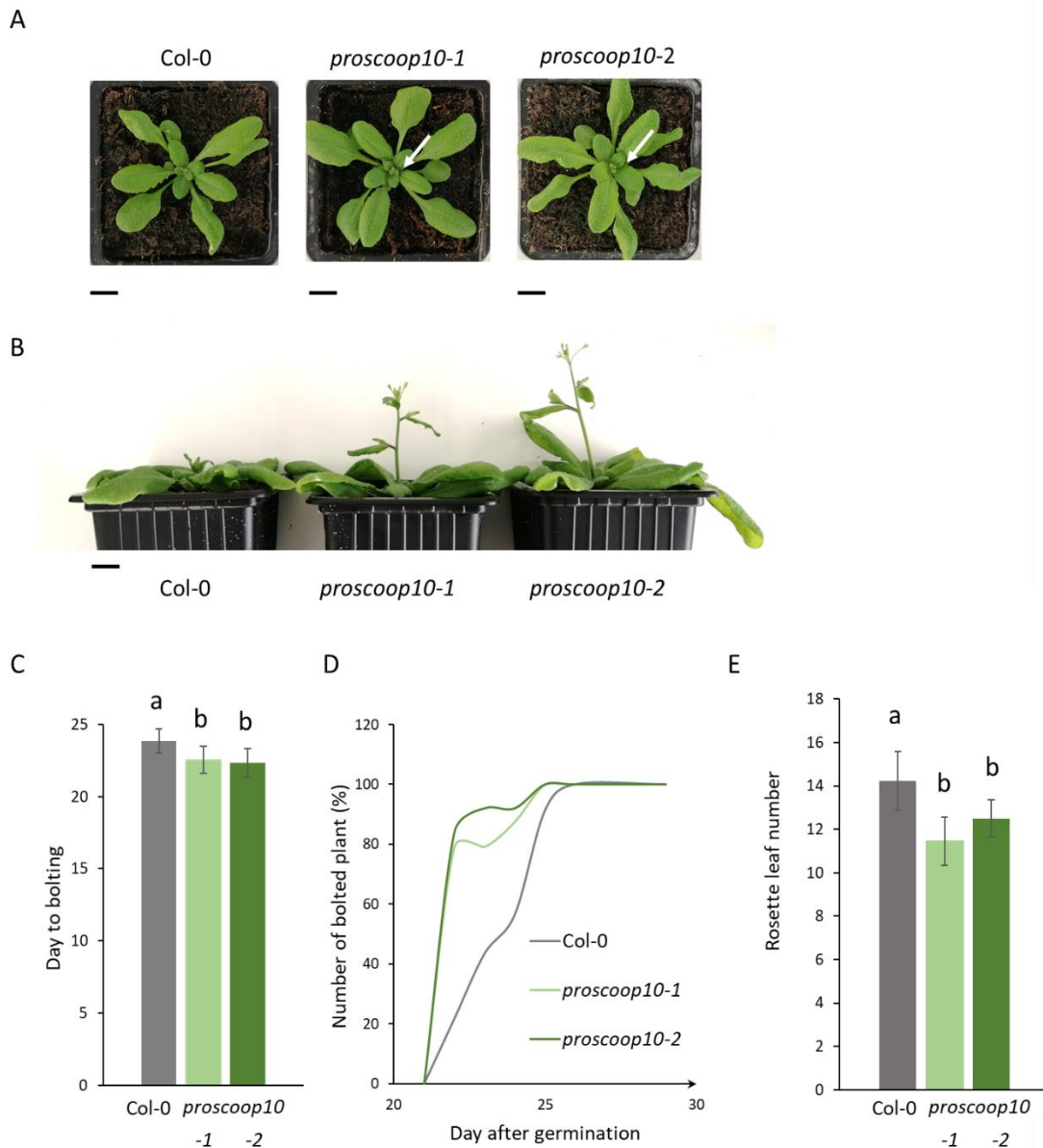


**Figure 5: *proscoop10* early flowering phenotype.**

(A) Bolted inflorescence of the *proscoop10* mutant lines, the 22<sup>nd</sup> day after germination, indicated by the white arrows. (B) Delay of stem development between mutants and WT due to the early flowering of the *proscoop10* lines, at the 27<sup>th</sup> day after germination. Scale bar = 1cm for (A) and (B). (C) Average of day to bolting for each genotype. (D) Kinetics represent the number of bolted inflorescences in %, starting from day 20 to day 30 after germination. (n=25). (E) Average of the number of rosette leaves at the flowering time for each genotype. For (C) and (E) ANOVA and Tukey test allowed to define significantly two different groups labelled a and b.

878

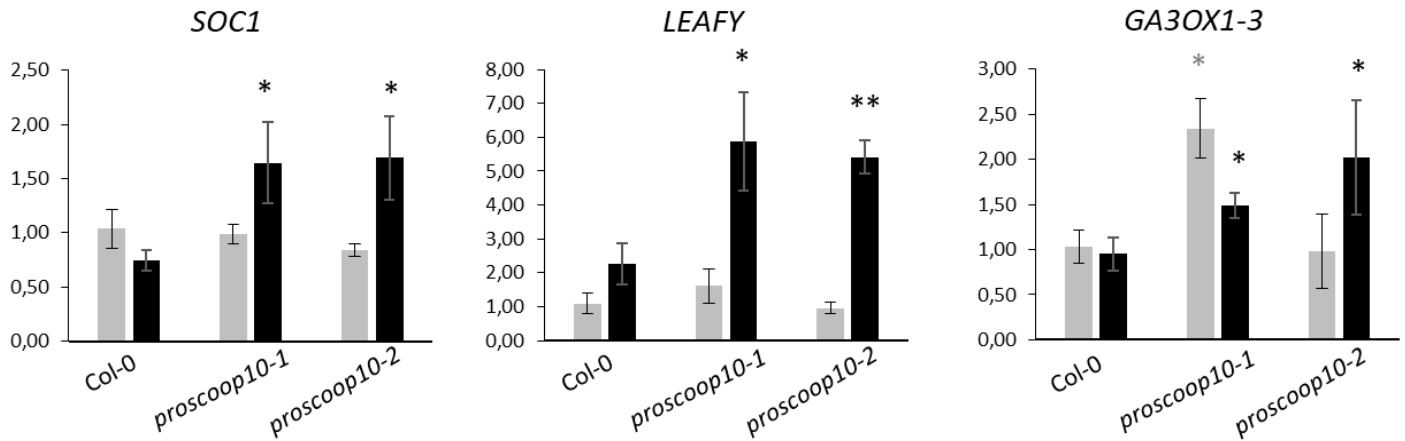


**Figure 6: Impact of *PROSCOOP10* mutation on transcription of genes involved in floral regulation**

Relative expression of *SOC1*, *LEAFY* and *GA3OX1-3* genes was measured by RT-qPCR after 7 days (in grey) and 11 days (in black) in the two *proscocoop10* mutant lines compared to Col-0 at 7 days. Values represent mean ratios  $\pm$  SEM of three independent biological replicates. Asterisks denote statistical differences of gene expression levels between *proscocoop10* mutants and Col-0 : \* $P < 0.05$ , \*\* $P < 0.01$  (ratio paired t-test).